

AN OVERVIEW OF GPS OCCULTATIONS FOCUSING ON RETRIEVING WATER VAPOR

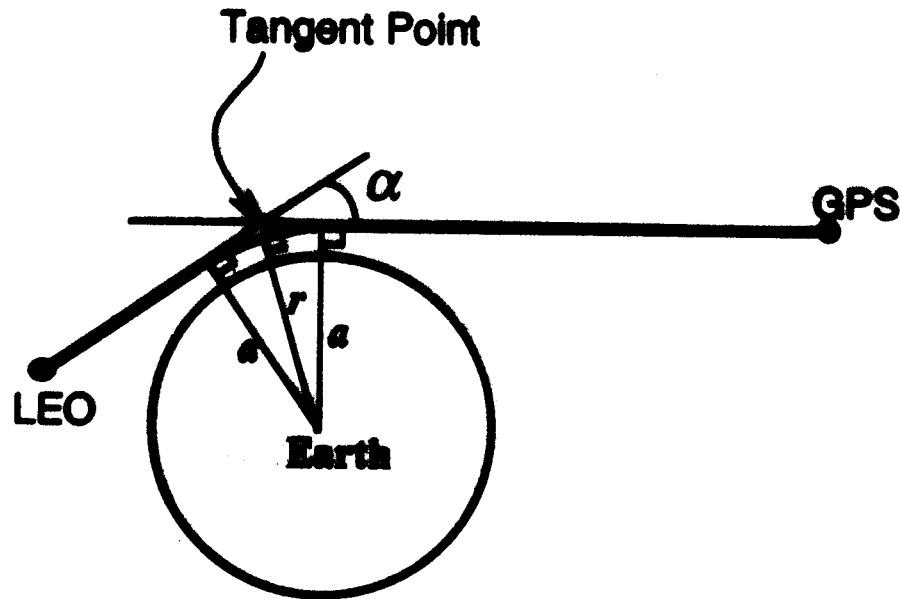
R. Kursinski

Jet Propulsion Laboratory
California Institute of Technology

October 20, 1999

International Symposium on GPS
October 18-22, 1999
Tsukuba, Ibaraki, Japan

OCCULTATION GEOMETRY AND THE ABEL TRANSFORM LEO OBSERVING A GPS SATELLITE



- Assuming spherical symmetry:

Forward propagation

Abel inversion

$$\alpha = -2a \int_{r_0}^{\infty} \frac{d \ln(n) / dr}{\sqrt{r^2 n^2 - a^2}} dr \quad \Rightarrow \quad \ln(n(r)) = \frac{1}{\pi} \int_{\infty}^{\infty} \frac{\alpha}{\sqrt{a^2 - r^2 n^2}} da$$

OBTAINING GEOPHYSICAL VARIABLES FROM REFRACTIVITY

$$N = (n-1) \times 10^6 = 77.6 \frac{P}{T} + 3.73 \times 10^5 \frac{P_w}{T^2} - 40.3 \times 10^6 \frac{n_e}{f^2} + \text{higher order ionospheric terms}$$

Dry Moist Ionosphere

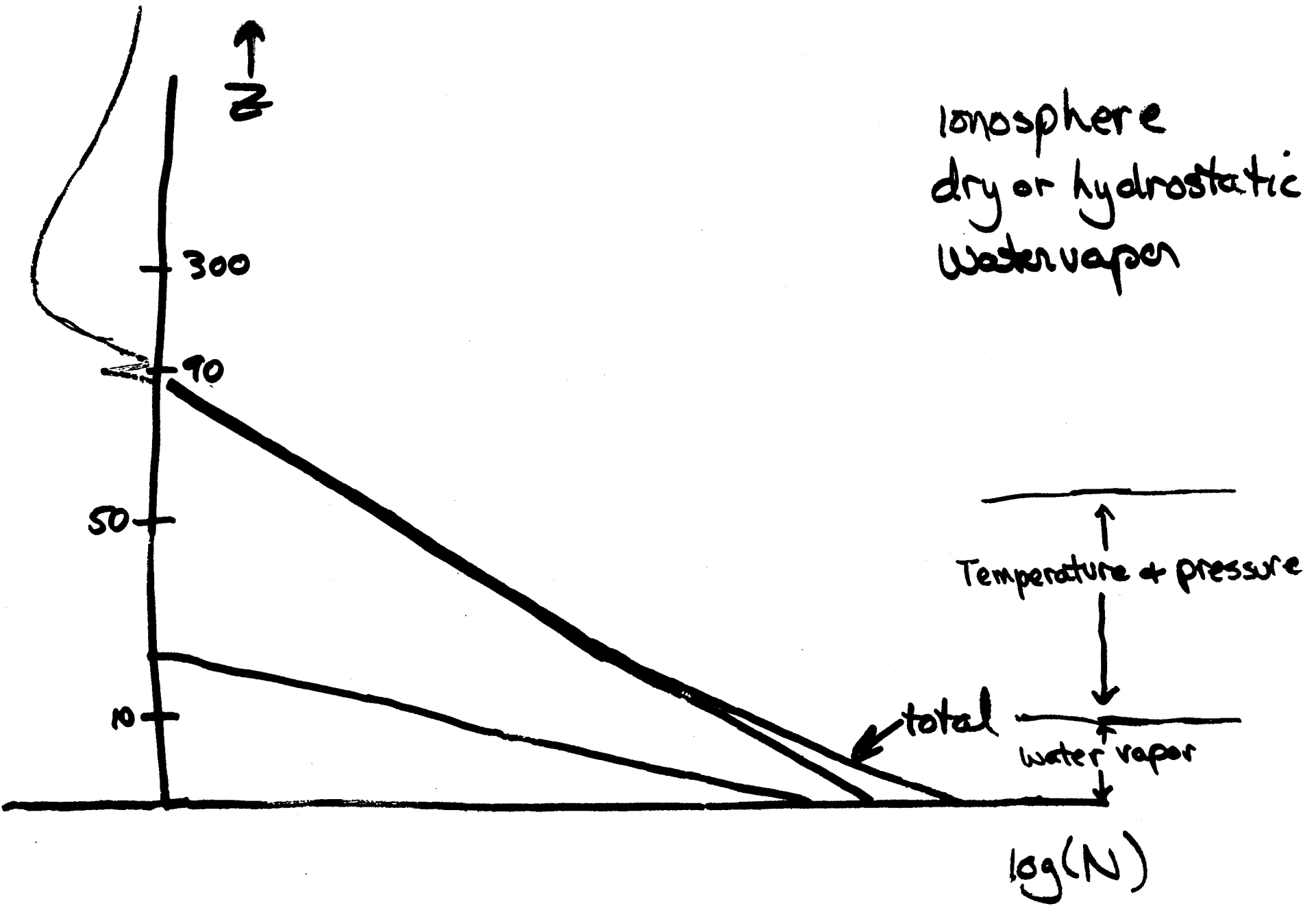
- Equation of state

$$\rho = 0.3484 \frac{P}{T}$$

- Hydrostatic equilibrium equation

$$\frac{\partial P}{\partial h} = -g\rho$$

n = index of refraction
 N = refractivity
 P = pressure
 T = temperature
 P_w = water vapor pressure
 n_e = electron density
 f = operating frequency
 ρ = density
 h = height
 g = gravitational acceleration



Key GPS Features

GPS constellation provides 24 occultation signal source at 20,000 km altitude and ~55° inclination

24 GPS sources plus a single GPS receiver in low Earth orbit yield 400 to 700 globally distributed, daily occultations

Small, simple, inexpensive and low power receiver instrumentation

Density of occultations increased by placing additional receivers (and transmitters) in orbit

Remote Sensing Characteristics

Simple technique

Very accurate measurement of atmospheric delay (1 part in 10^6 near surface)

Low optical depth and insensitivity to condensed water at ~20 cm wavelengths

High vertical resolution of Fresnel diffraction (~1 km)

=> Accurate, routine limb sounding of troposphere

Observations provide very accurate temperature and geopotential estimates in stratosphere and cold troposphere ($T < 250$ K)

Observations should yield accurate estimates of water vapor in the warmer regions of the mid-to lower troposphere

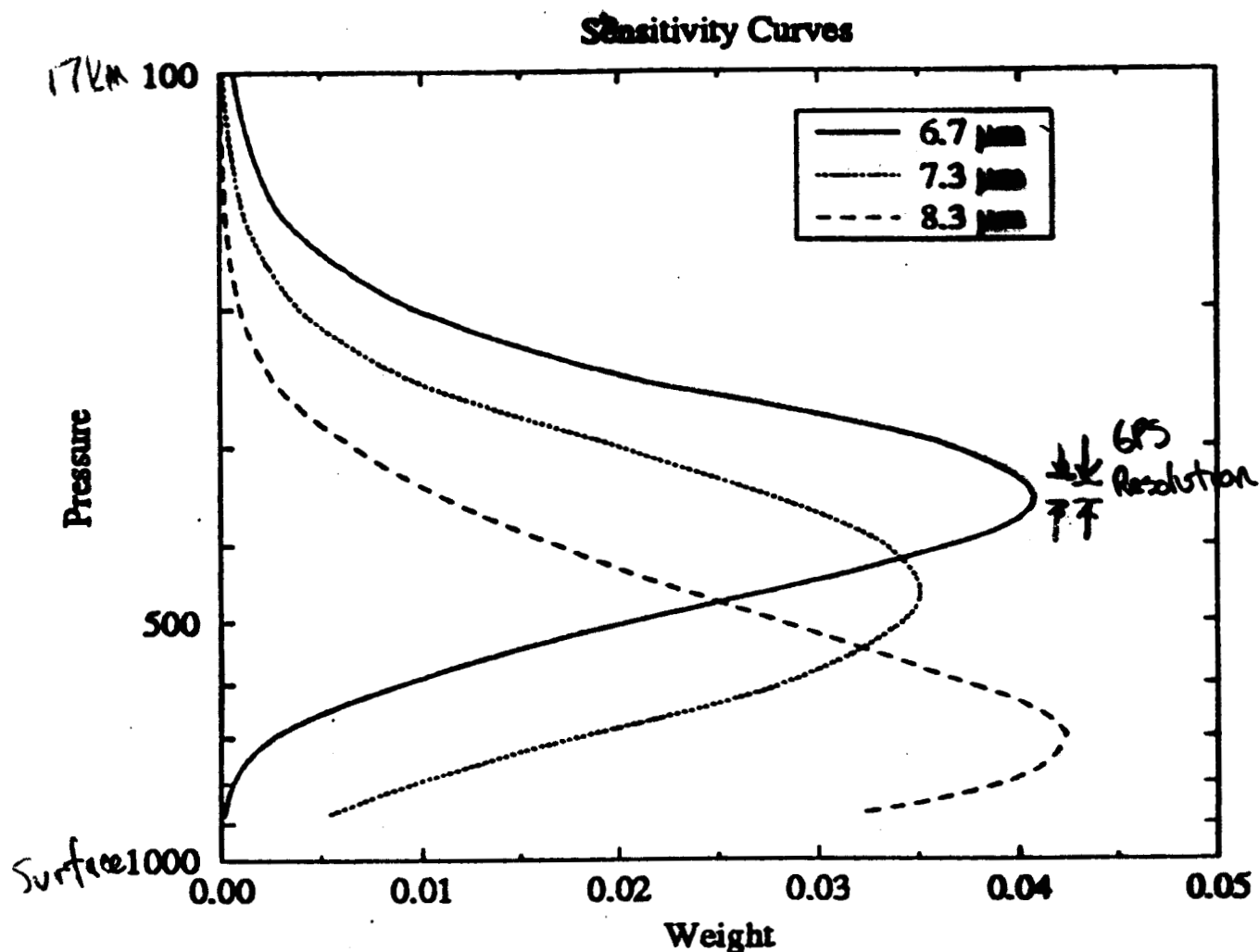


Figure 1. Sensitivity of $T_{6.7}$ (solid), $T_{7.3}$ (dotted), and $T_{8.3}$ (dashed) to local perturbations in relative humidity in thin layers equally spaced in the logarithm of pressure ($\Delta \ln p = dp/p \approx 0.04$). The curves are normalized such that the sum of weights over pressure is equal to unity.

corresponding clear-sky radiosonde climatology containing the identical sampling restrictions present in the satellite data. This study suggested that the restriction to clear and partially cloudy conditions introduces a slight dry bias into the TOVS climatology, typically about 4% and usually less than 10% when expressed in terms of the relative humidity. We note, however, that these results were heavily weighted toward the

humid inter
organ
of the
SB93.
transf
and lo
sensiti
of the
tropos
conclu

2. Results

This study used a humid reader facility to facilitate the radian transfer function for broad-band TOVS channels. The irregular sampling of the model was addressed by using independent model lines. The idealized and diabatic nature of the radiosonde climatology was idealized and diabatically corrected. The radiance sensitivities were calculated for the temperature

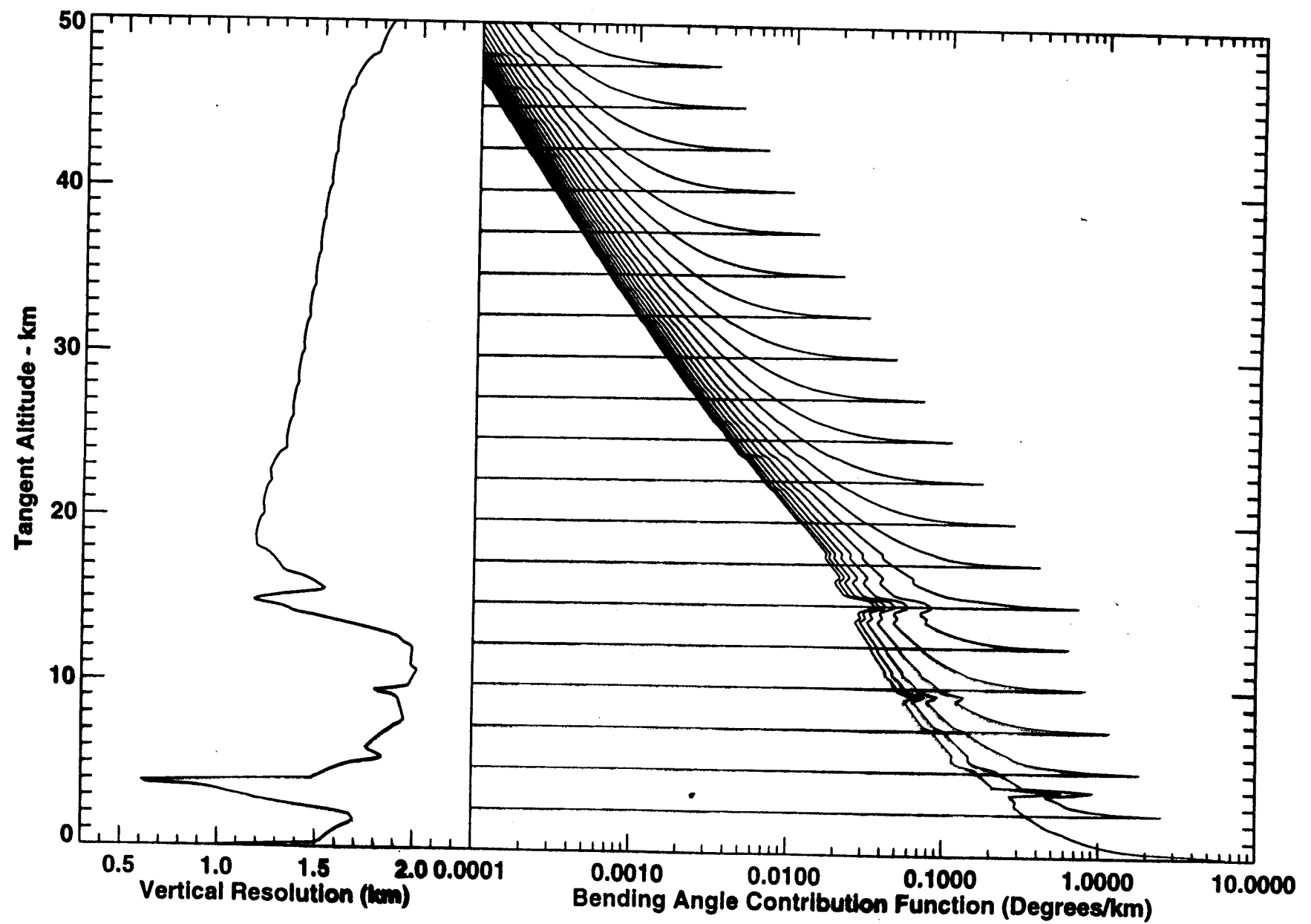
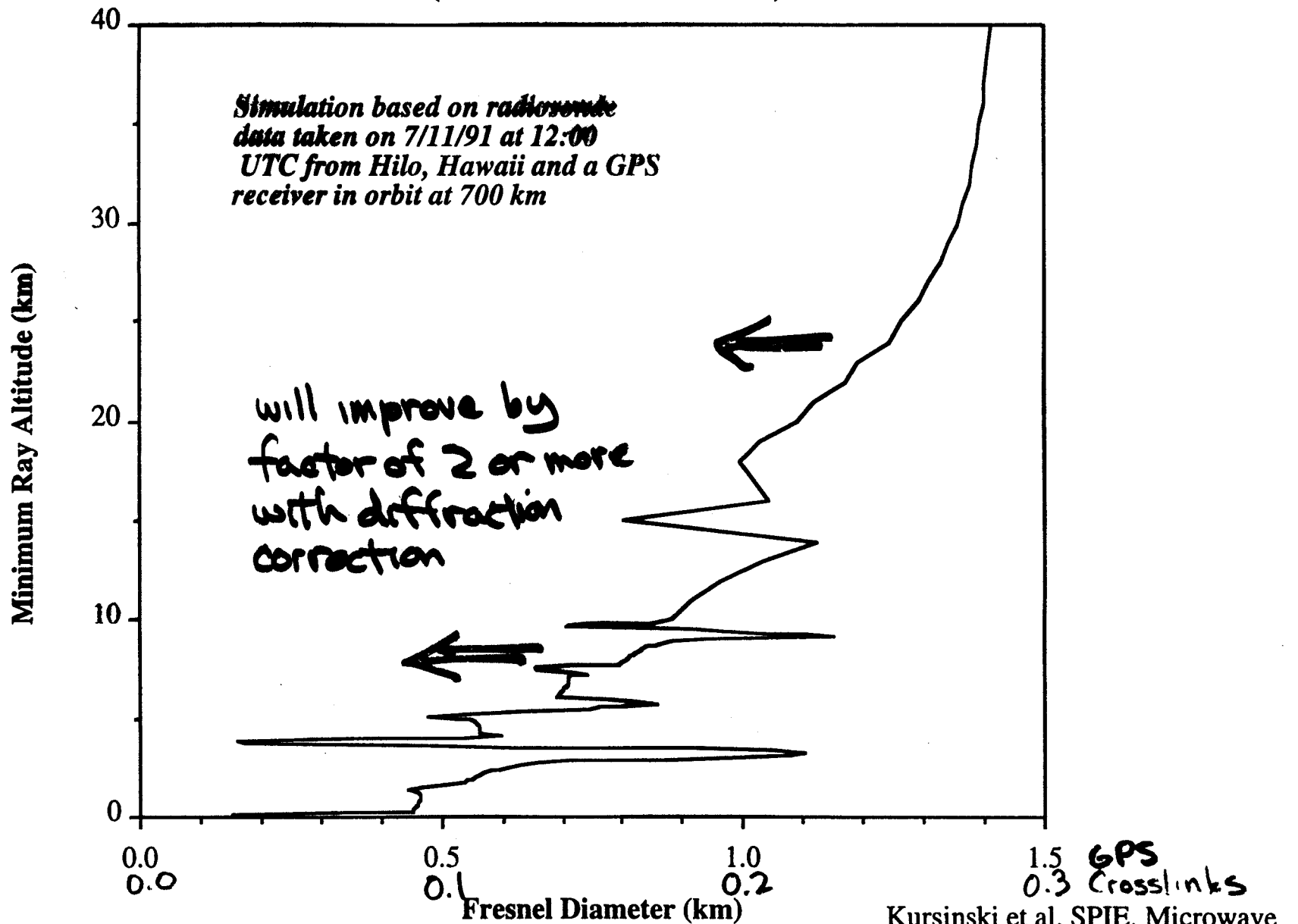


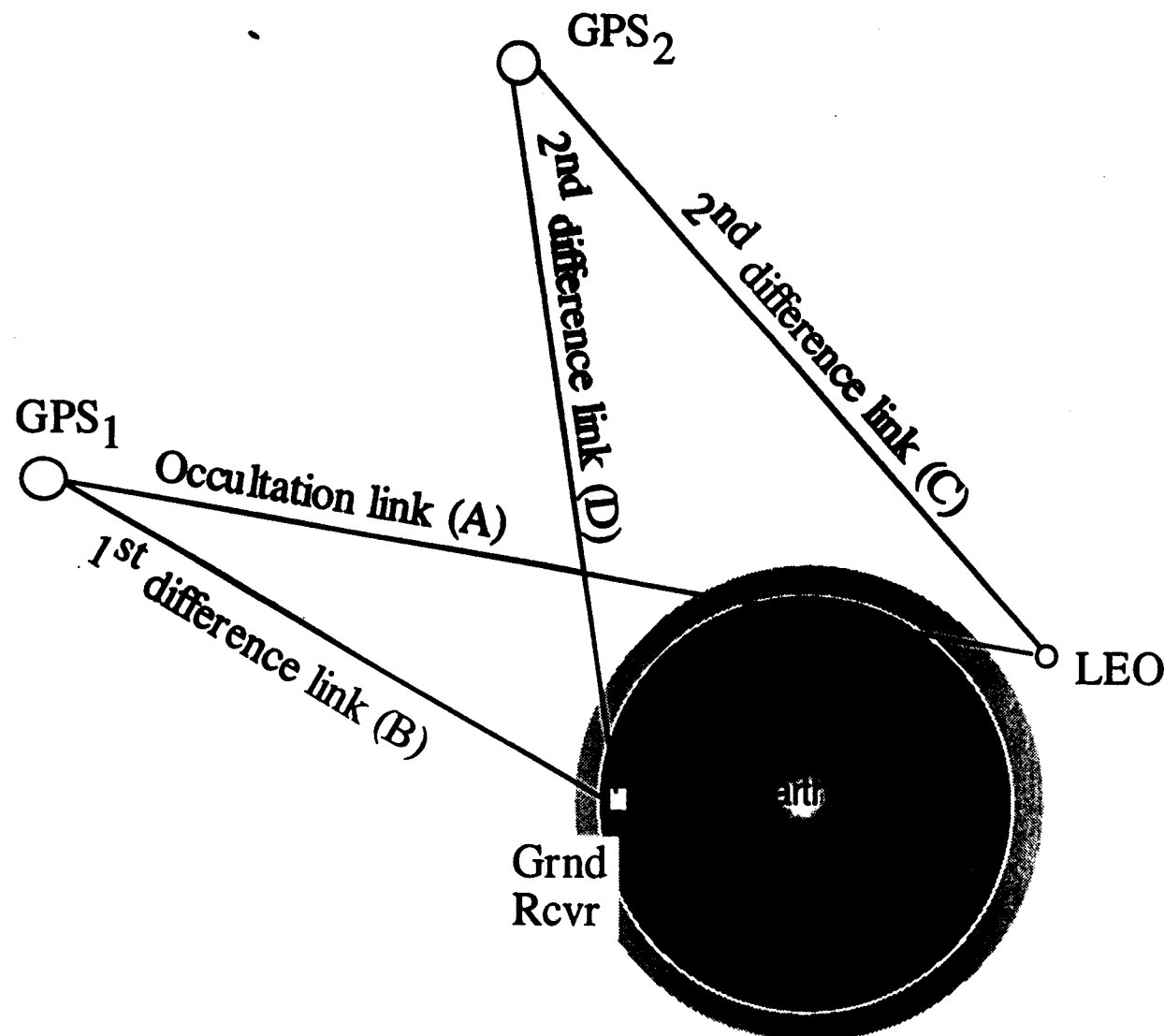
Figure 8

Vertical Resolution (Fresnel Zone Diameter)



Kursinski et al. SPIE, Microwave
Instrumentation for Remote
Sensing of the Earth, April 1993

Ground Network: Geometry for calibrating clock errors



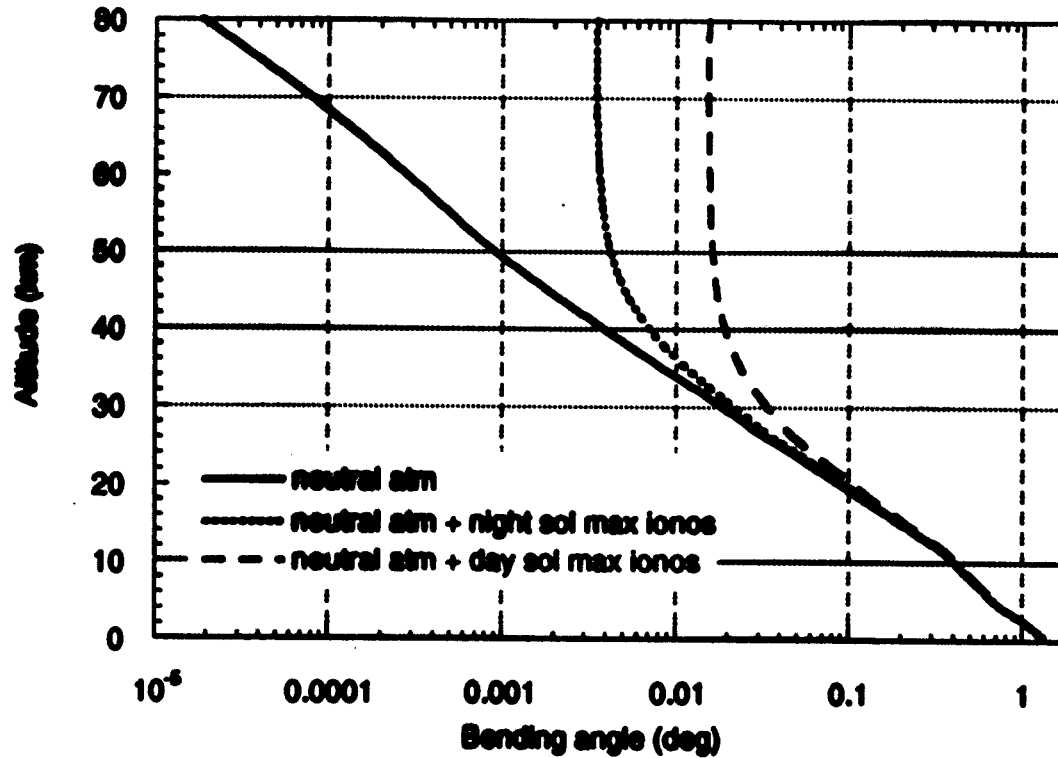


Figure 2.6. Atmospheric and ionospheric bending for limb ray paths plotted as a function of ray path tangent height. Solid line: bending calculated for U.S. Standard Atmosphere (Champion et al., 1985). Long dashed line: bending calculated for U.S. standard atmosphere plus typical mid-latitude ionosphere during daytime, solar maximum conditions. Short dashed line: bending calculated for U.S. standard atmosphere plus typical mid-latitude ionosphere during nighttime, solar maximum conditions.

Ionosphere Calibration

GPS has two signal frequencies to calibrate the dispersive ionospheric refractivity, $\sim 1/f^2$, where f is the radio signal frequency.

Upward Looking Receiver:

- The ionosphere free path length is $L = c_i L_1 - (c_i - 1) L_2$

where L is the optical path length along a signal path defined as

$$L_{opt} = \int_{path} n dl = \int_{path} (1 + N) dl$$

L_1 and L_2 are the optical path lengths at the two GPS signal frequencies, 1.57542 and 1.2276 GHz respectively
the coefficient, $c_i = (1 - \frac{f^2}{f_i^2})^{-1}$ equals 2.5457...

Occultation Receiver:

- The ionosphere-free bending is

$$\alpha_{neutral}(a) = c_i \alpha_1(a) - (c_i - 1) \alpha_2(a) \quad (1)$$

where α_1 and α_2 are the total bending angles for the two GPS signal frequencies.

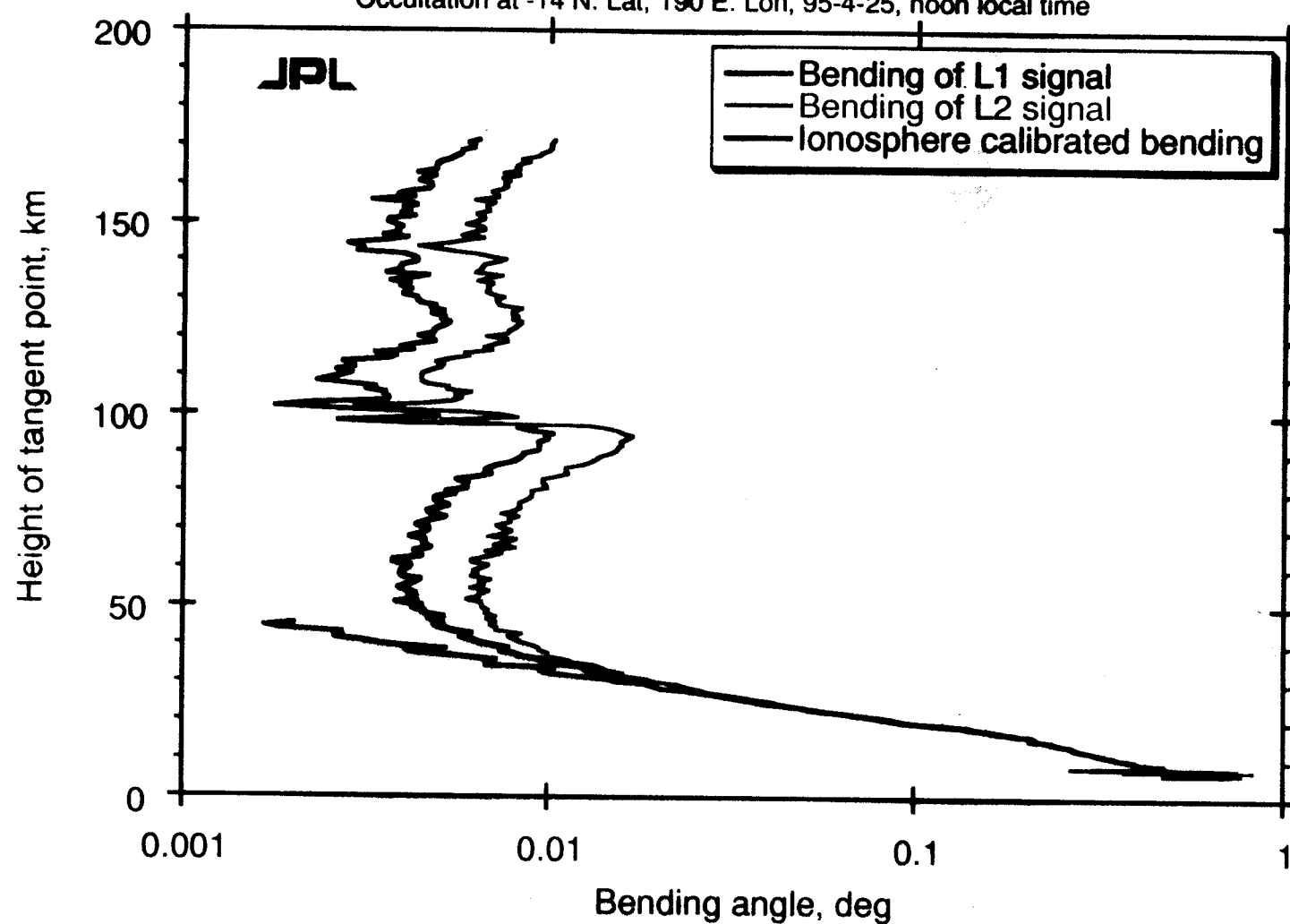
- In the occultation geometry, the dispersive refractivity causes the two GPS signal paths to separate.
- An solution developed by Vorob'ev and Krasil'nikova [1993] based on separating the charge-neutral atmosphere and ionospheric bending angle contributions (assuming a spherically symmetric index of refraction) :

$$\alpha(a) = 2 a \int_{r_0}^{\infty} \frac{\frac{dn_{neut}}{dr} dr}{n_{neut} \sqrt{(n_{neut} r)^2 - a^2}} + 2 a \frac{40.3}{f^2} \int_{r_0}^{\infty} \frac{\frac{dn_e}{dr} dr}{n_{neut} \sqrt{(n_{neut} r)^2 - a^2}}$$

- Application of (1) requires interpolation from the discrete set of $\alpha_2(a_2)$ to the set of a_1 values.

Bending of signal as a function of height from surface

Occultation at -14 N. Lat, 190 E. Lon, 95-4-25, noon local time



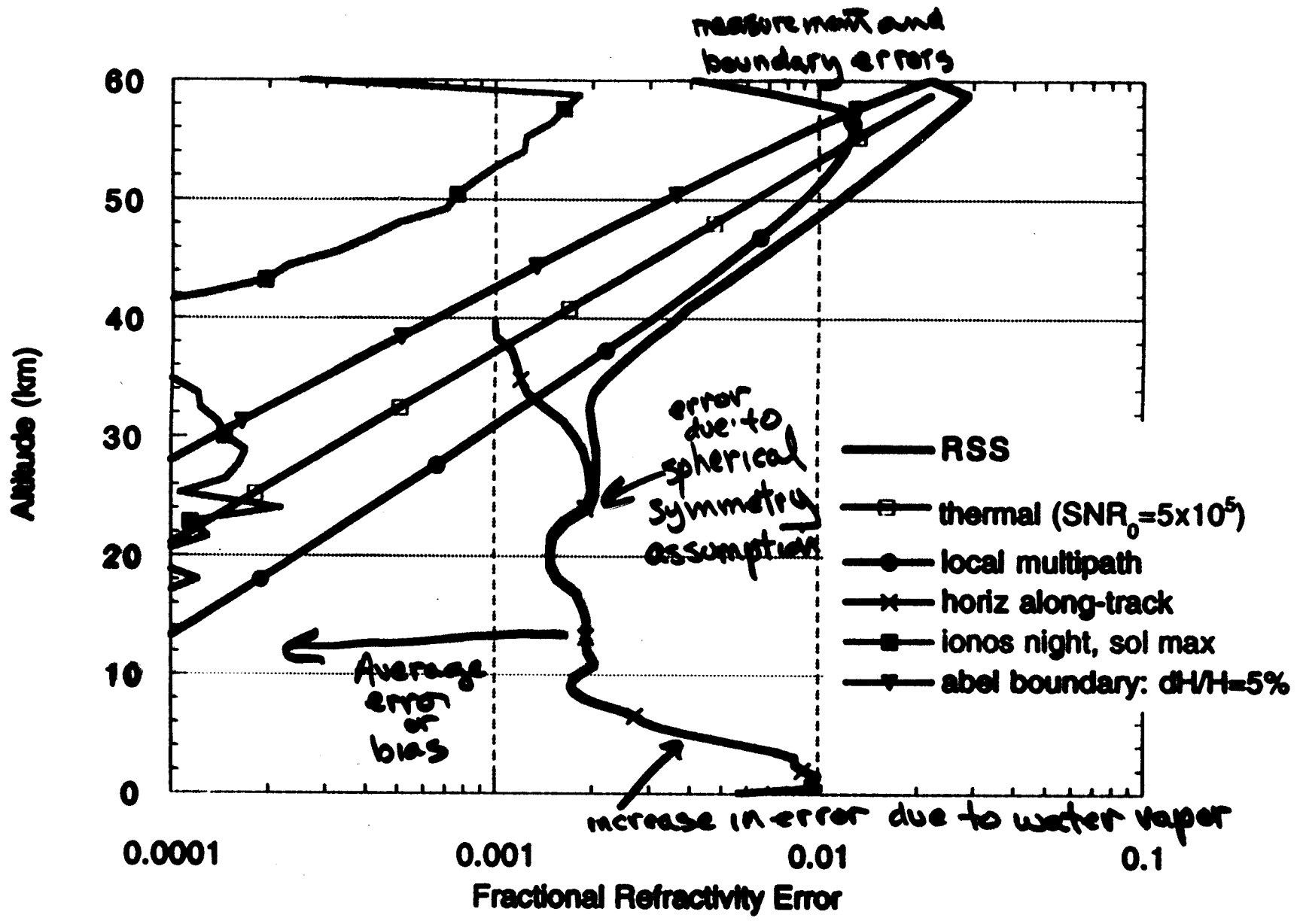


Figure 18

Kurianski et al., 1999? Observing Earth's atmosphere

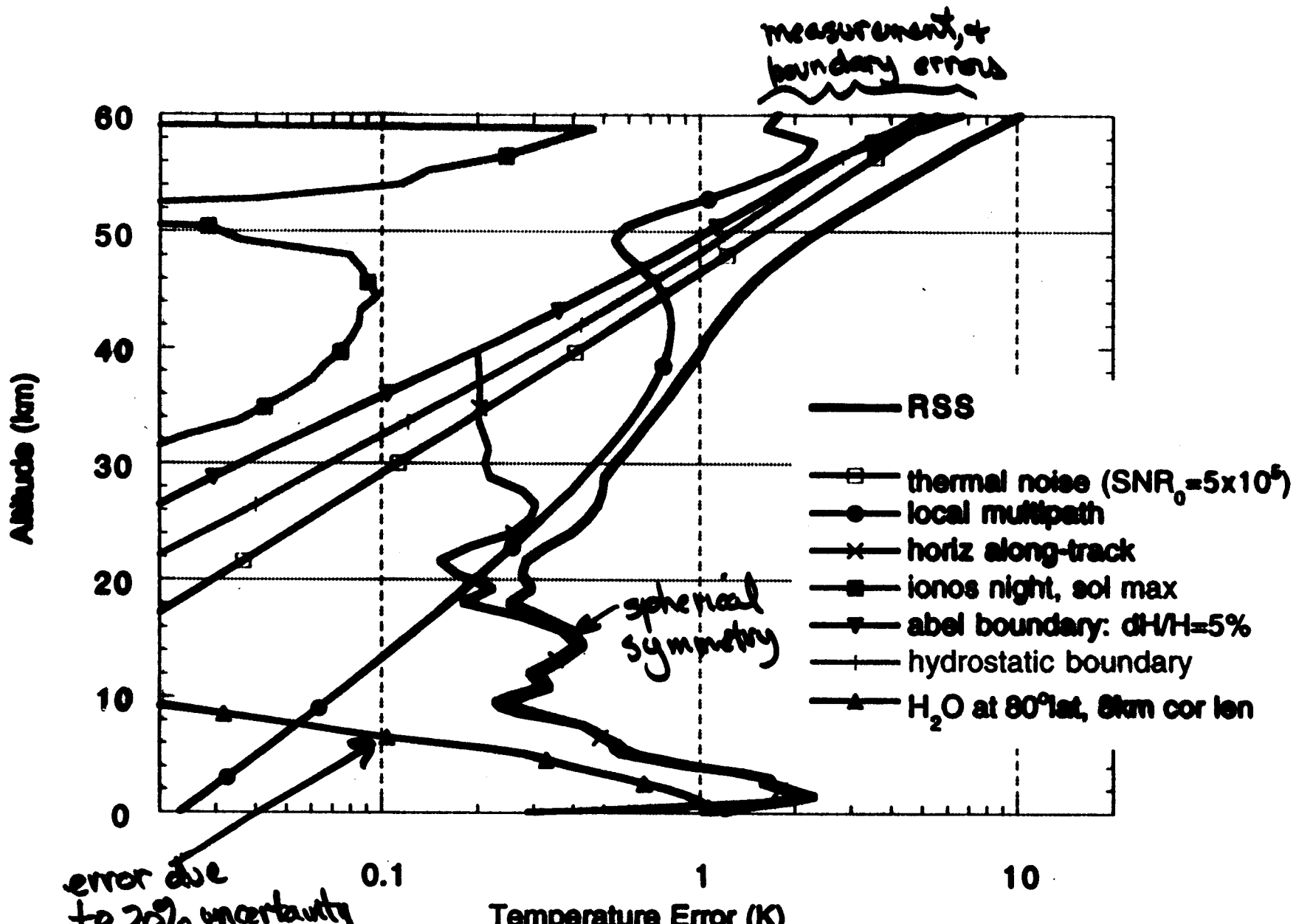
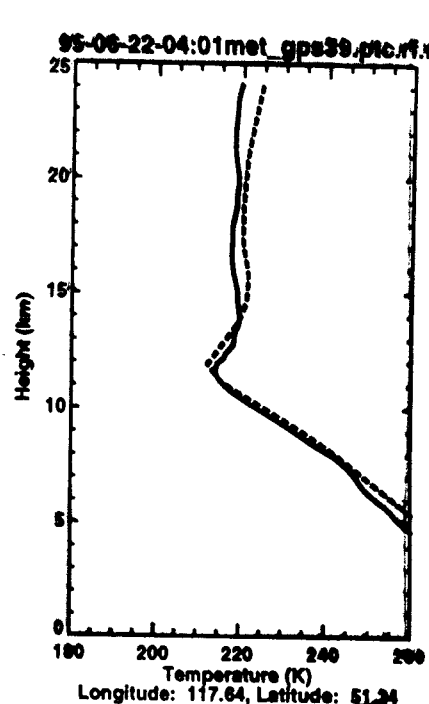
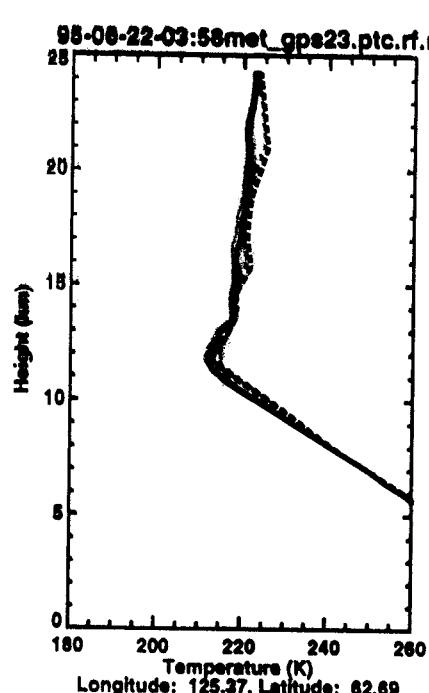
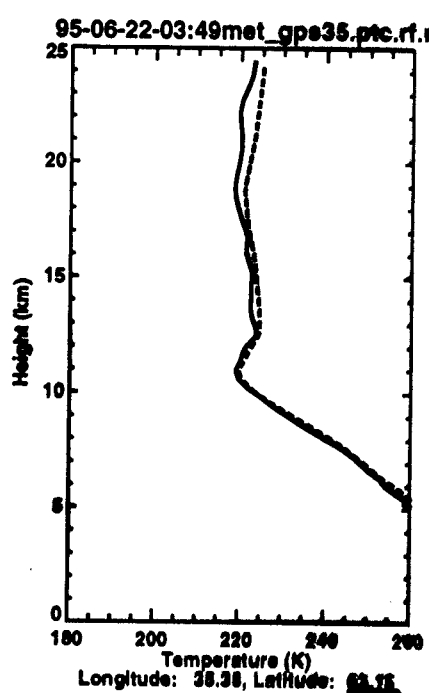
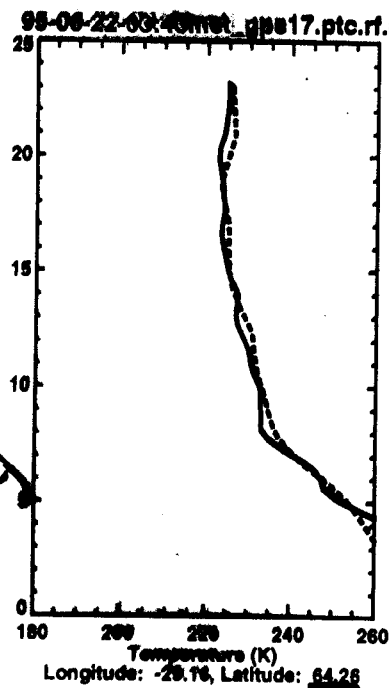


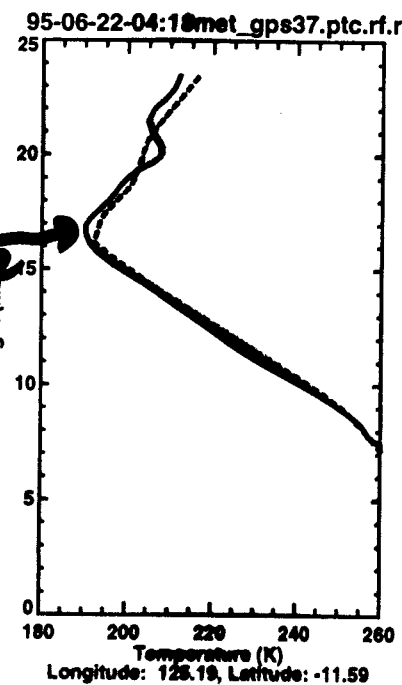
Figure 20

Kursinski et al., 1995 ?
Observing Earth's atmosphere

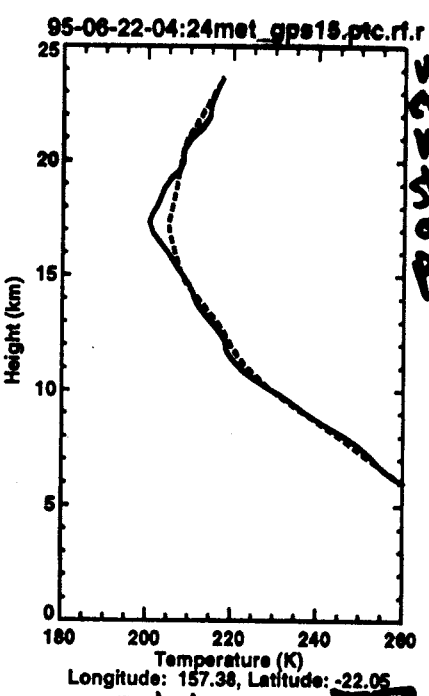
high
northern
latitude
(summer)



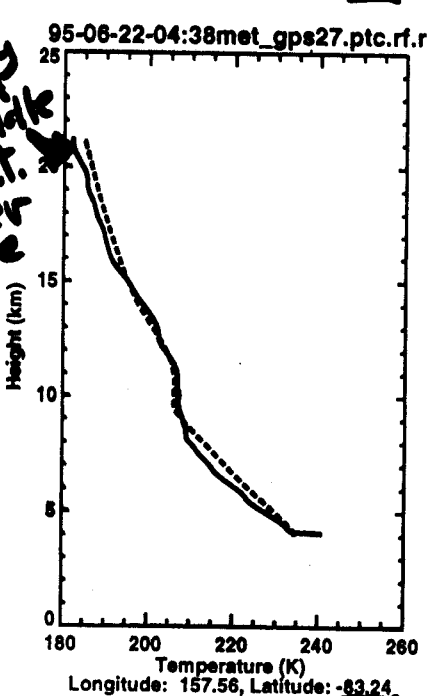
cold
tropical
tropopause



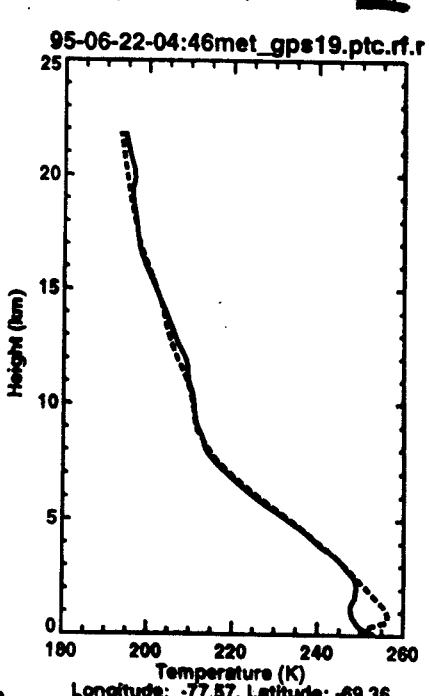
TROPICAL



Subtropical



very
cold
middle
strat.
over
pole



High Southern Latitude (WINTER)

Figure 6.5 8 profiles from June 22, 1995 demonstrating the range of temperature structure observed by GPS-MET
Solid lines are occultation profiles. Dashed lines are interpolated from ECMWF analyses

EQUATORIAL WAVES

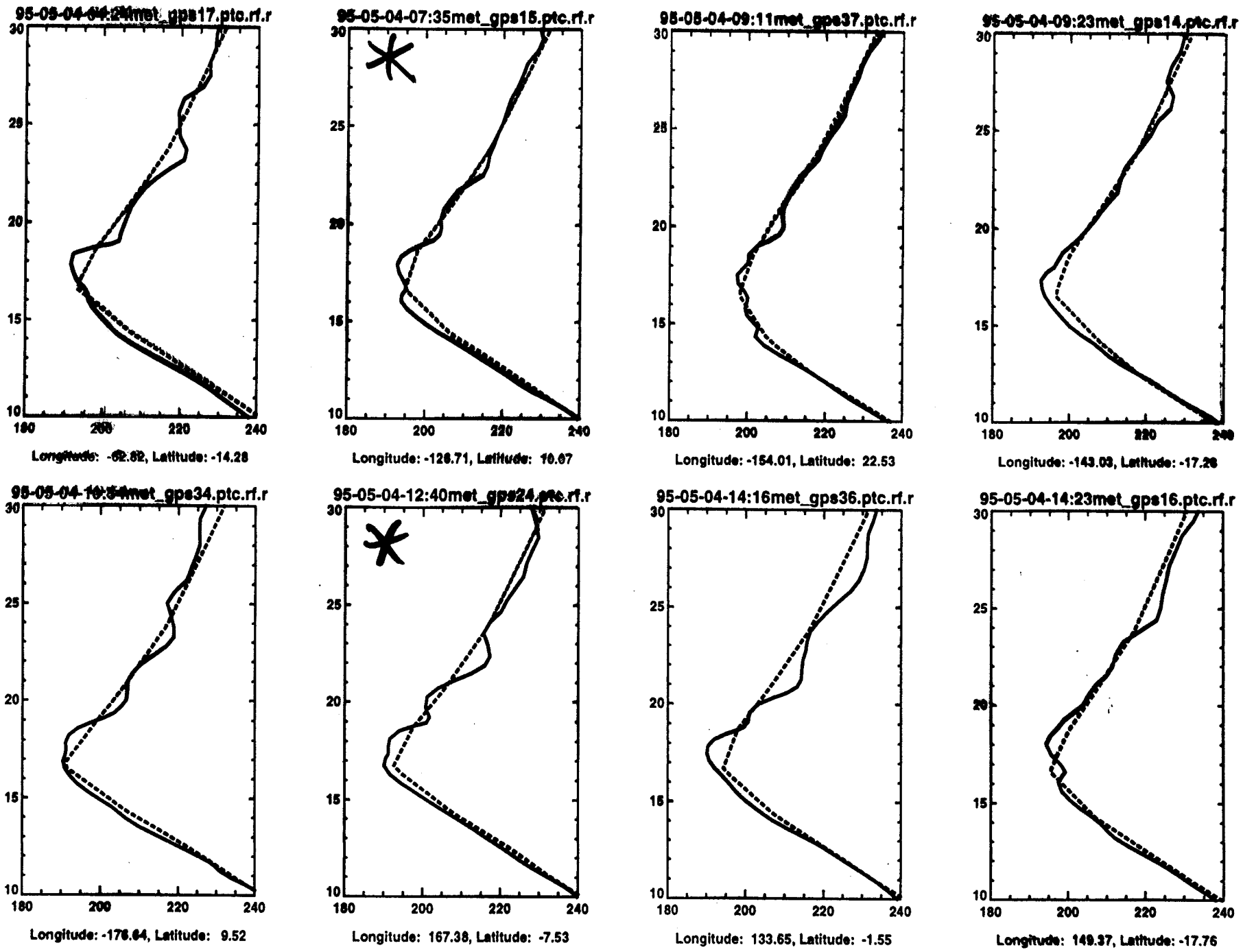
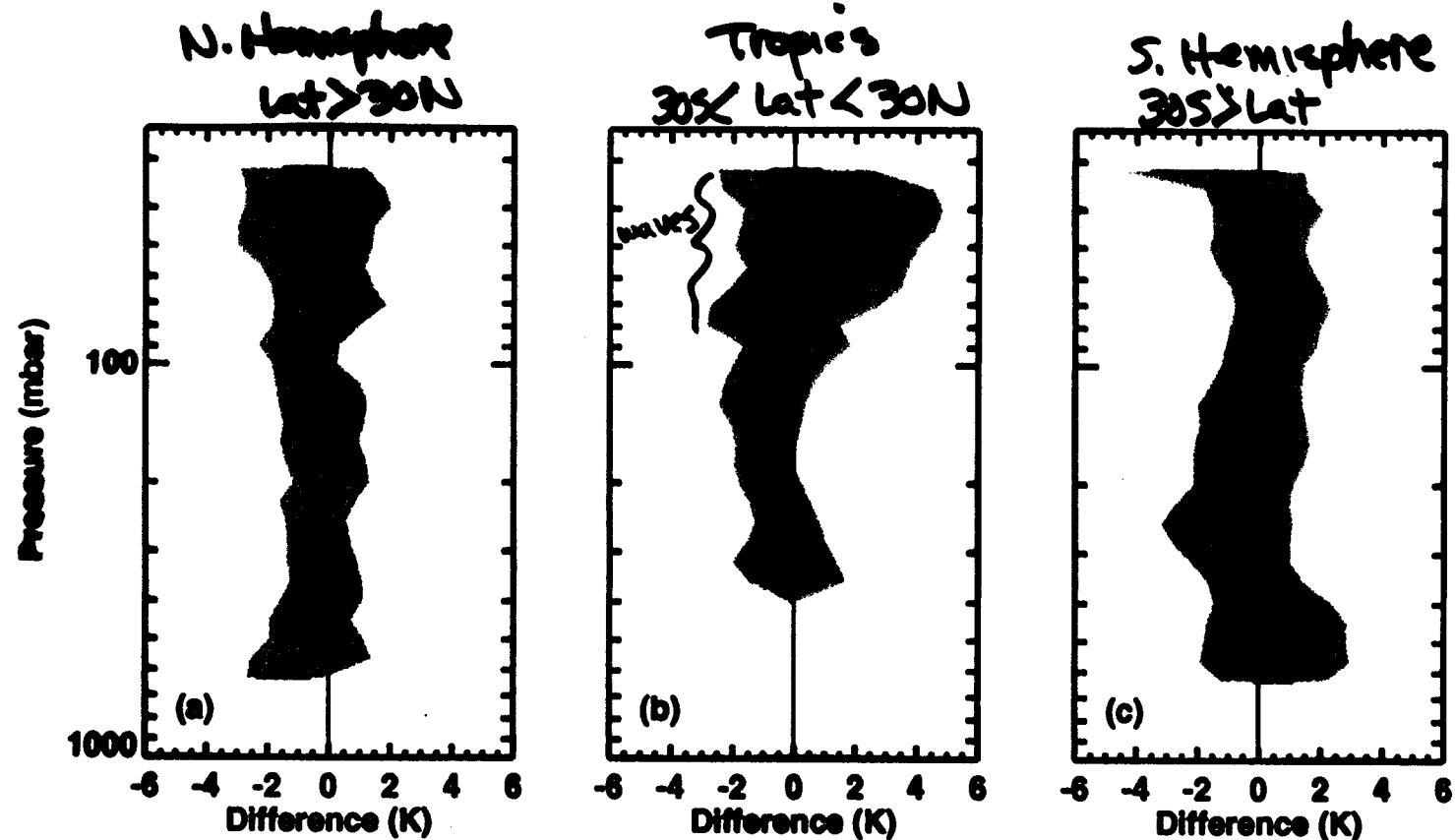


Figure 6.6 Examples of low latitude temperature profiles. Solid lines of occultation profiles. Dashed lines are interpolated from daily NMC stratosphere analyses

5.1

TEMPERATURE DIFFERENCES
Apr.-May 1995 OCC - ECMWF GLOBAL ANALYSIS



KURSINSKI et al.
SCIENCE, 271, 1107 (1996)

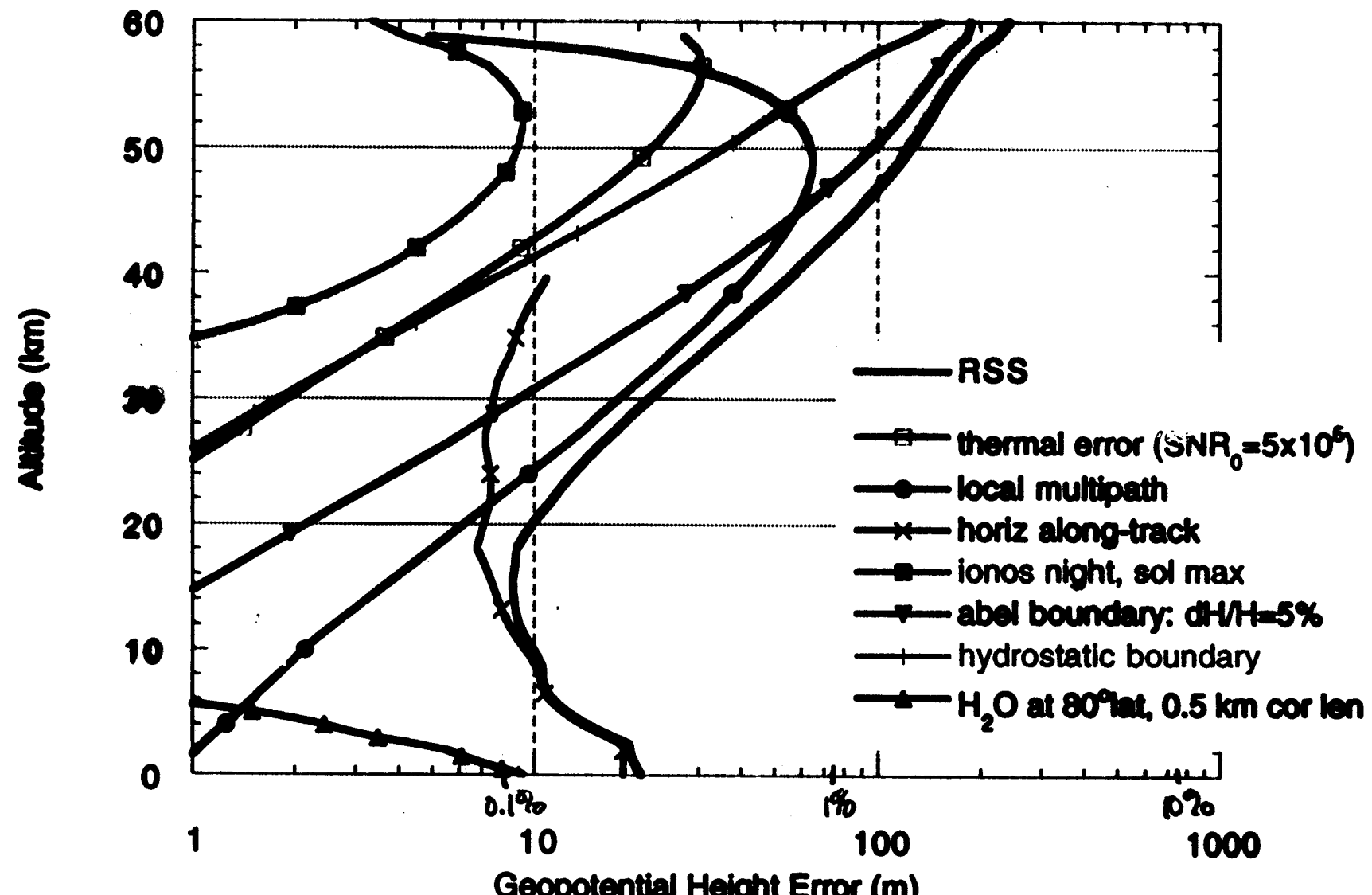
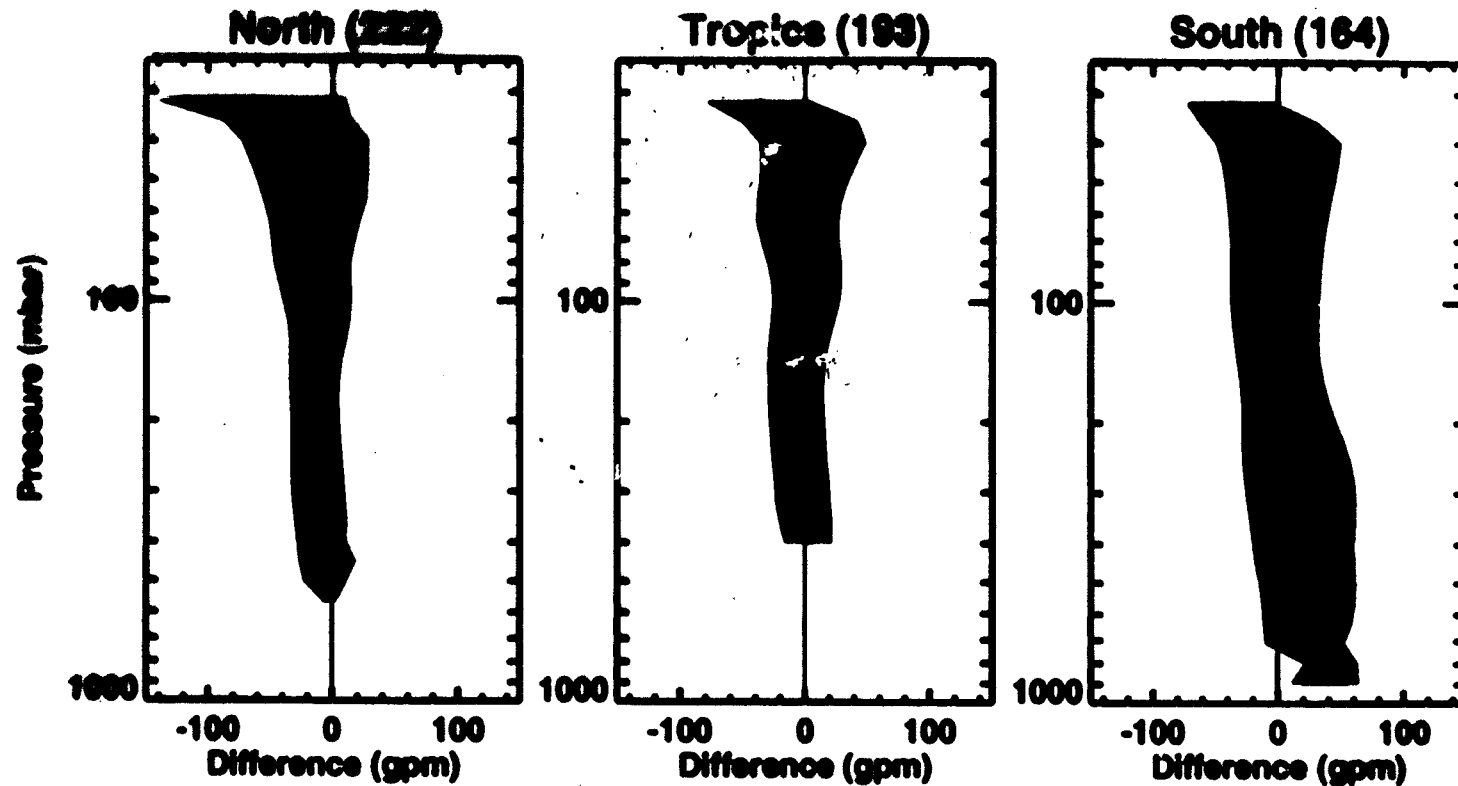


Figure 19

Kursinski et al., 1996
Observing Earth's atmosphere

Comparison of GPS/MET Retrievals to ECMWF

Summer AS-off Period



JPL: Kursinski, Hajj, Bertiger, Leroy, Romans, Schofield, et al. (12 March 1996)

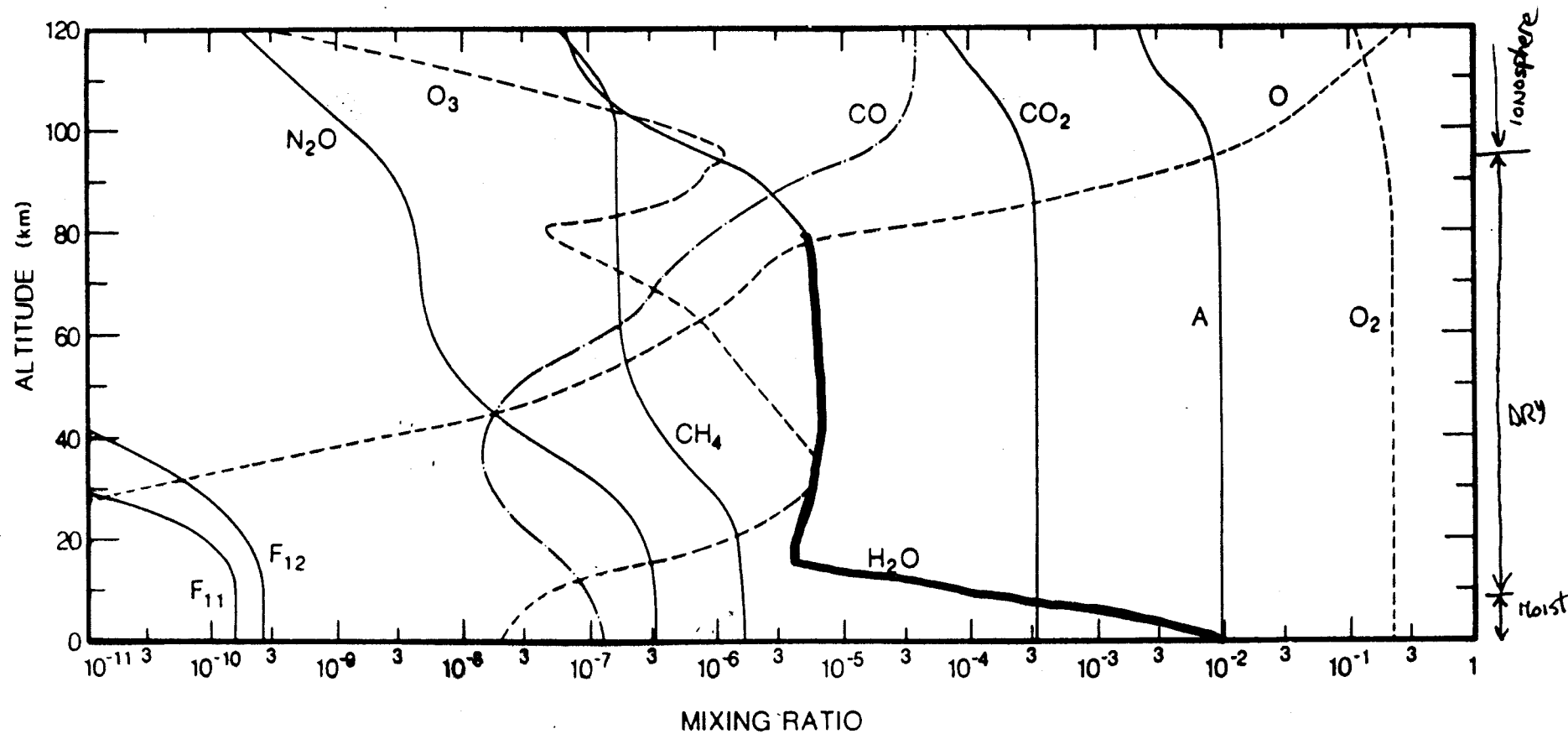


FIG. 1.5. Vertical profiles of mixing ratio of selected species at equinox. After Allen et al. (1981, 1984).

Estimated Accuracy of Specific Humidity

NOT
RELATIVE
HUMIDITY

- Specific humidity (water vapor mass mixing ratio):

$$q = \left[\frac{m_d}{m_w} \left(\frac{P}{P_w} - 1 \right) + 1 \right]^{-1}$$

- Changes in q , pressure P , temperature T and retrieved refractivity N are related:

$$dq = (C + q) \frac{dN}{N} + (C + 2q) \frac{dT}{T} - (C + q) \frac{dP}{P}$$

where C is $77.6 T m_w / 3.73e5 m_d$ [$C = 32 \text{ g/kg}$ at 230 K , $= 39 \text{ g/kg}$ at 300 K]

- Assuming independent errors in N , T and the surface pressure, P_s , yields

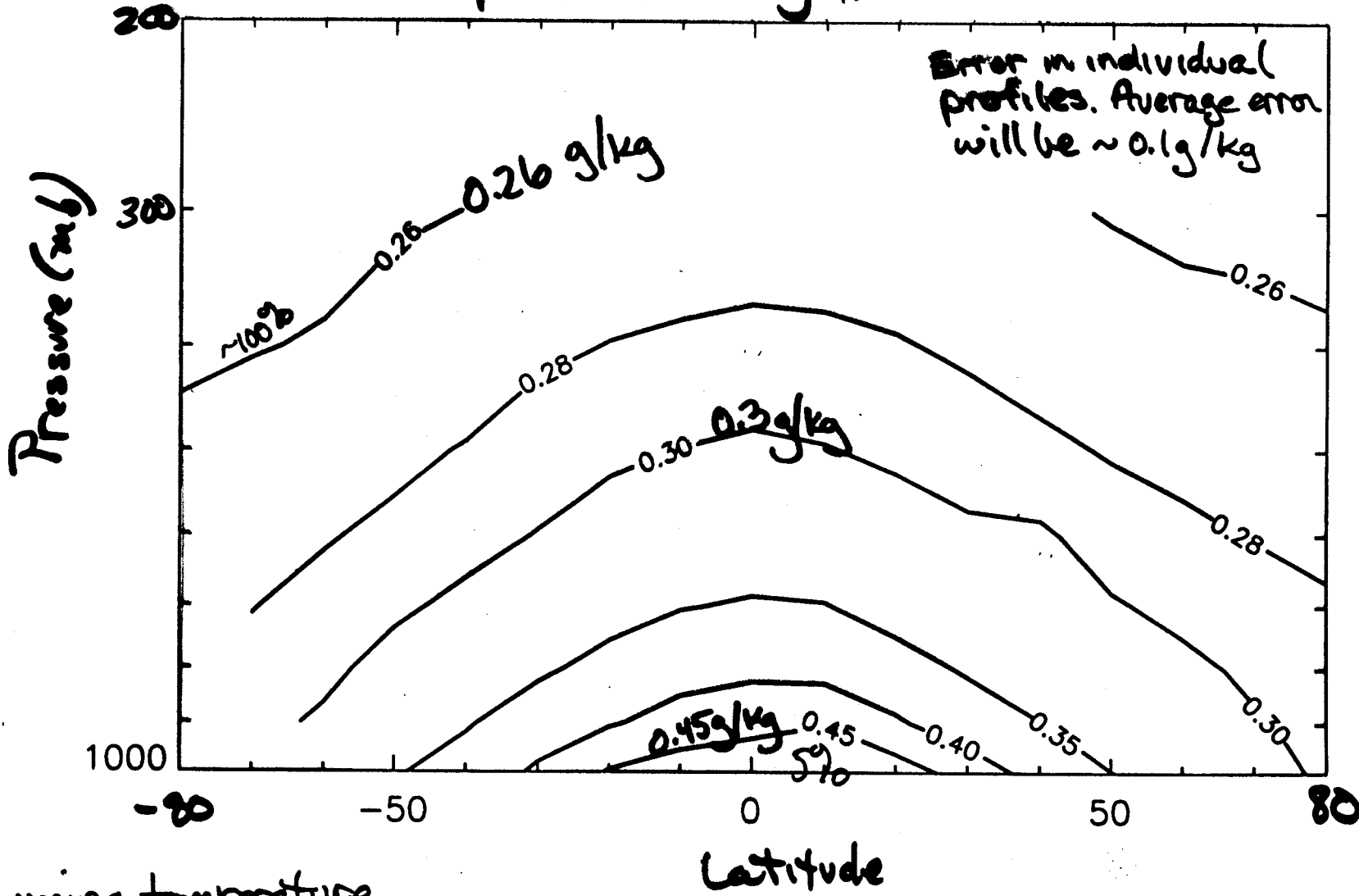
$$\sigma_q = \left[(C + q)^2 \left(\frac{\sigma_N}{N} \right)^2 + (C + 2q)^2 \left(\frac{\sigma_T}{T} \right)^2 + (C + q)^2 \left(\frac{\sigma_{P_s}}{P_s} \right)^2 \right]^{1/2}$$

- RMS error in q varies little ranging from 0.2 to 0.5 g/kg

- Higher altitude q error dominated by the T error ($\sim 1.5 \text{ K}$)
- Near surface q error has largest contribution by N error ($\sim 1\%$)
- Mean specific humidity, \bar{q} , accuracy is limited by mean T error

$$(\epsilon_T \sim 0.5 \text{ K} \Rightarrow \epsilon_q \sim 0.1 \text{ g/kg})$$

Error in Specific Humidity from 6 GPS Occultations



Assuming temperature
is known to $\sim 1.5 \text{ K}$

Refractivity error of
0.2% at 300 mb & above
1% near surface

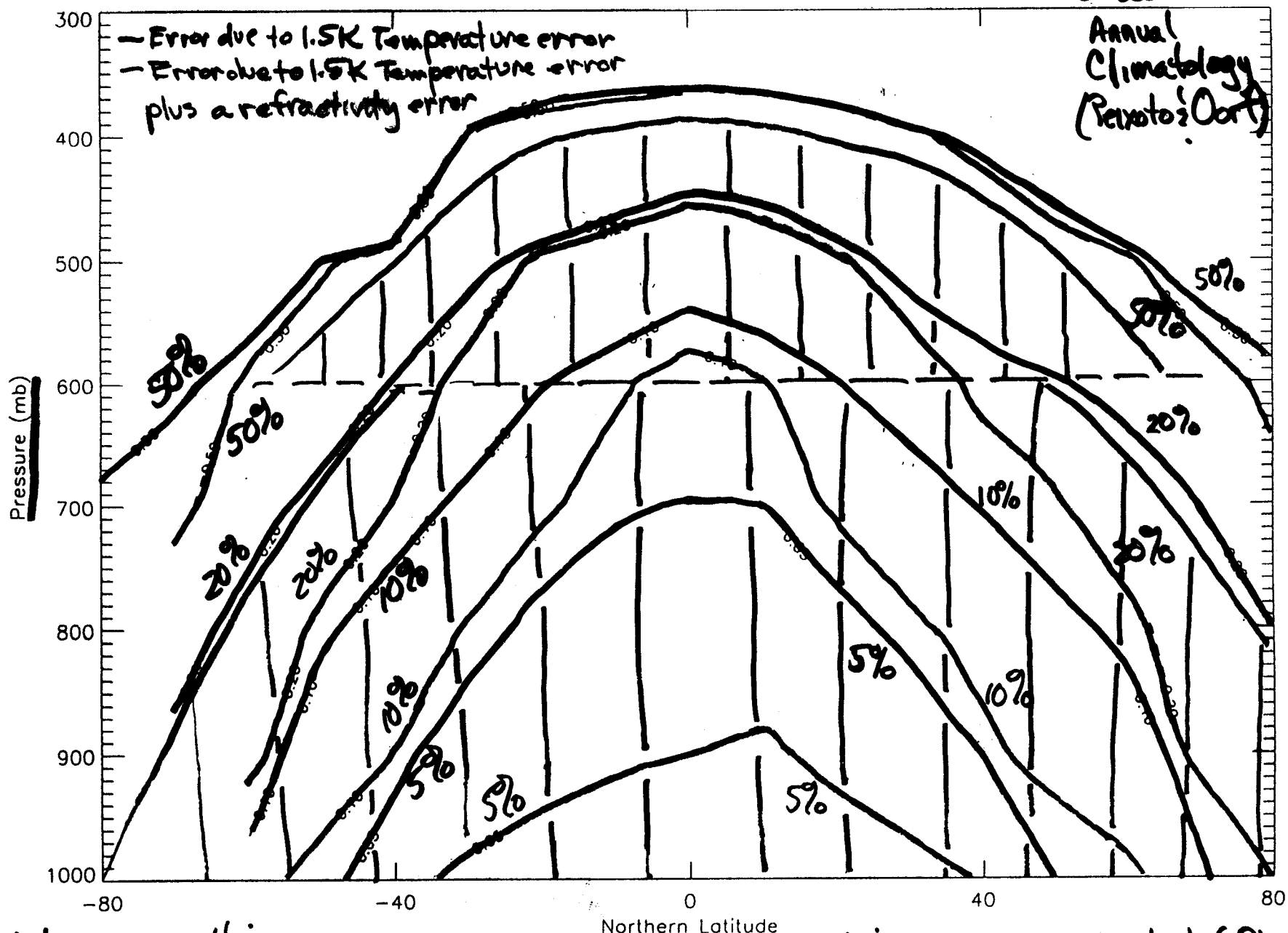
Figure 0

Kursinski & Hajj
An Examination of Water Vapor...
JGR 5/99

EXPECTED ACCURACY OF WATER VAPOR
DERIVED FROM GPS OCCULTATIONS

Based on:

Annual
Climatology
(Reynolds?)

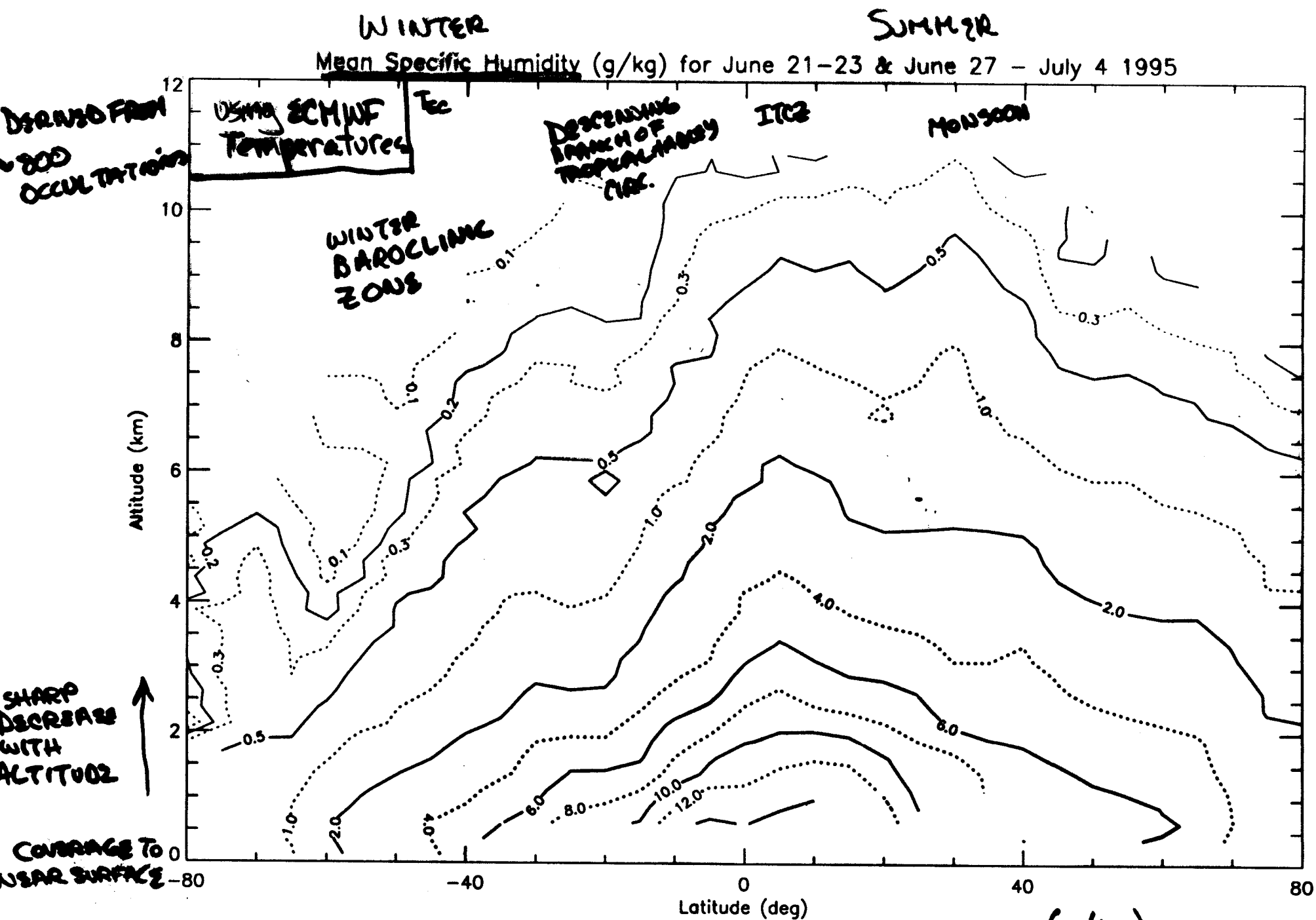


red shaded region is within
NPoESS specs.

— divide by $\sqrt{3}$ to get representative
estimate of climatological

Kursinski et al. GRL 1995

ERL 12/96



MEAN WATER VAPOR MIXING RATIO (g/kg)
DERIVED FROM GPS REFRACTIVITY; ECHWF TEMPERATURES

NOTE
North-South
asymmetry in
tropical Hadley
circulation

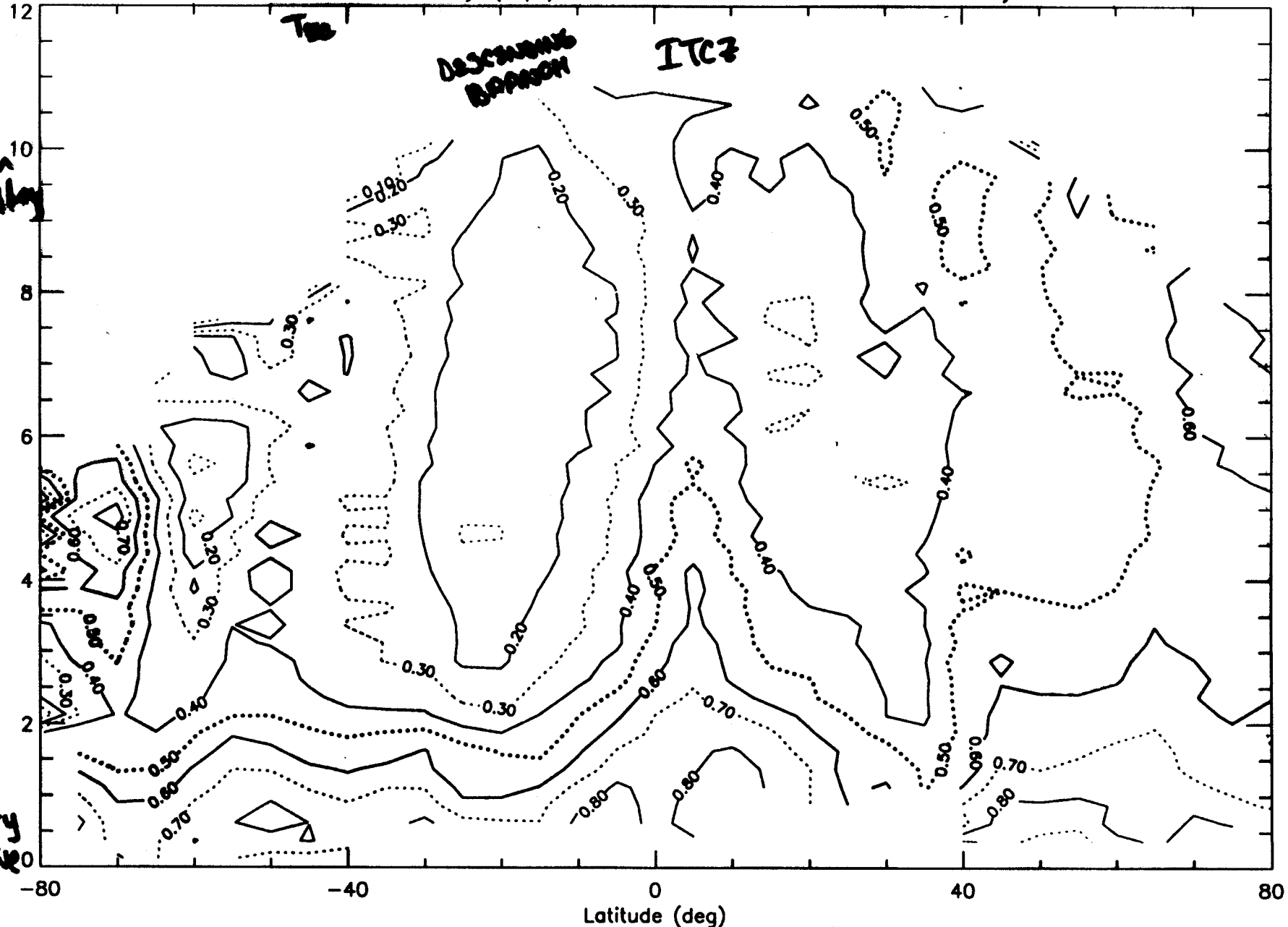
WINTER

SUMMER

Mean Relative Humidity (liq2) for June 21–23 & June 27 – July 4 1995

Altitude (km)

high boundary
layer relative
humidity

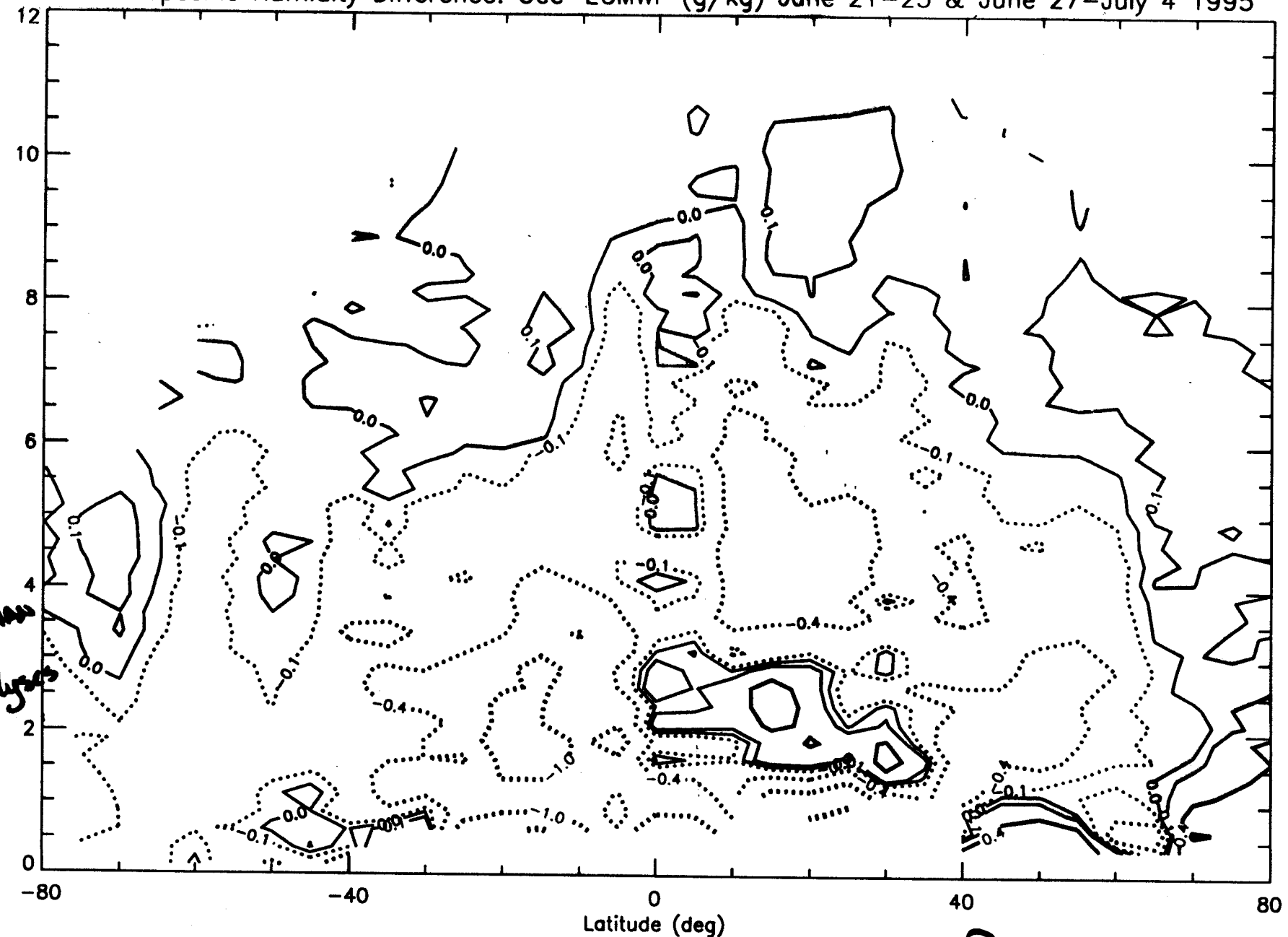


ZONAL MEAN RELATIVE HUMIDITY
(over liquid)

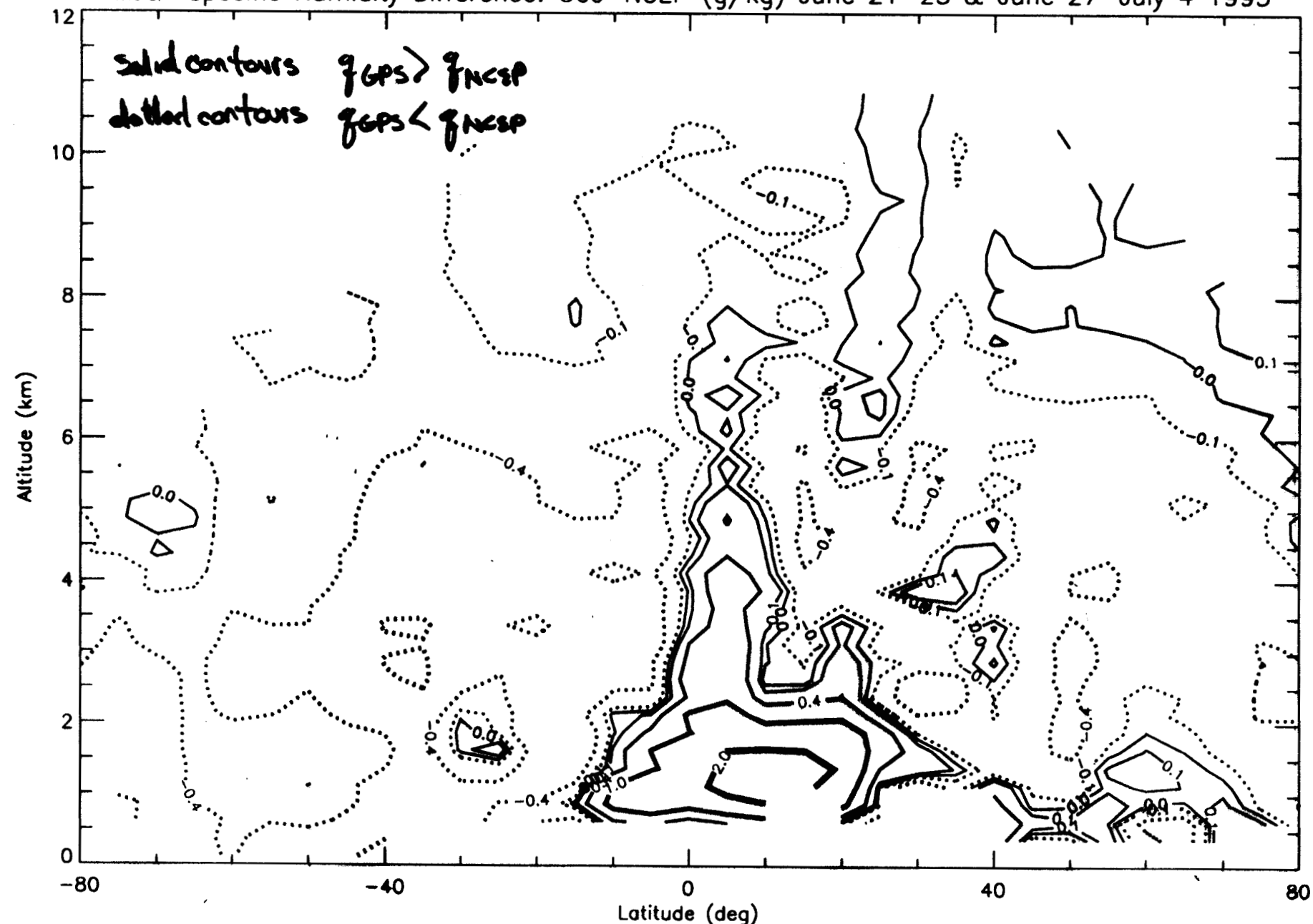
Kursinski & Hajj
1999

Mean Specific Humidity Difference: Occ-ECMWF (g/kg) June 21-23 & June 27-July 4 1995

*Most of the
transports
are DRIER THAN
THE ECMWF
humidity analyses*



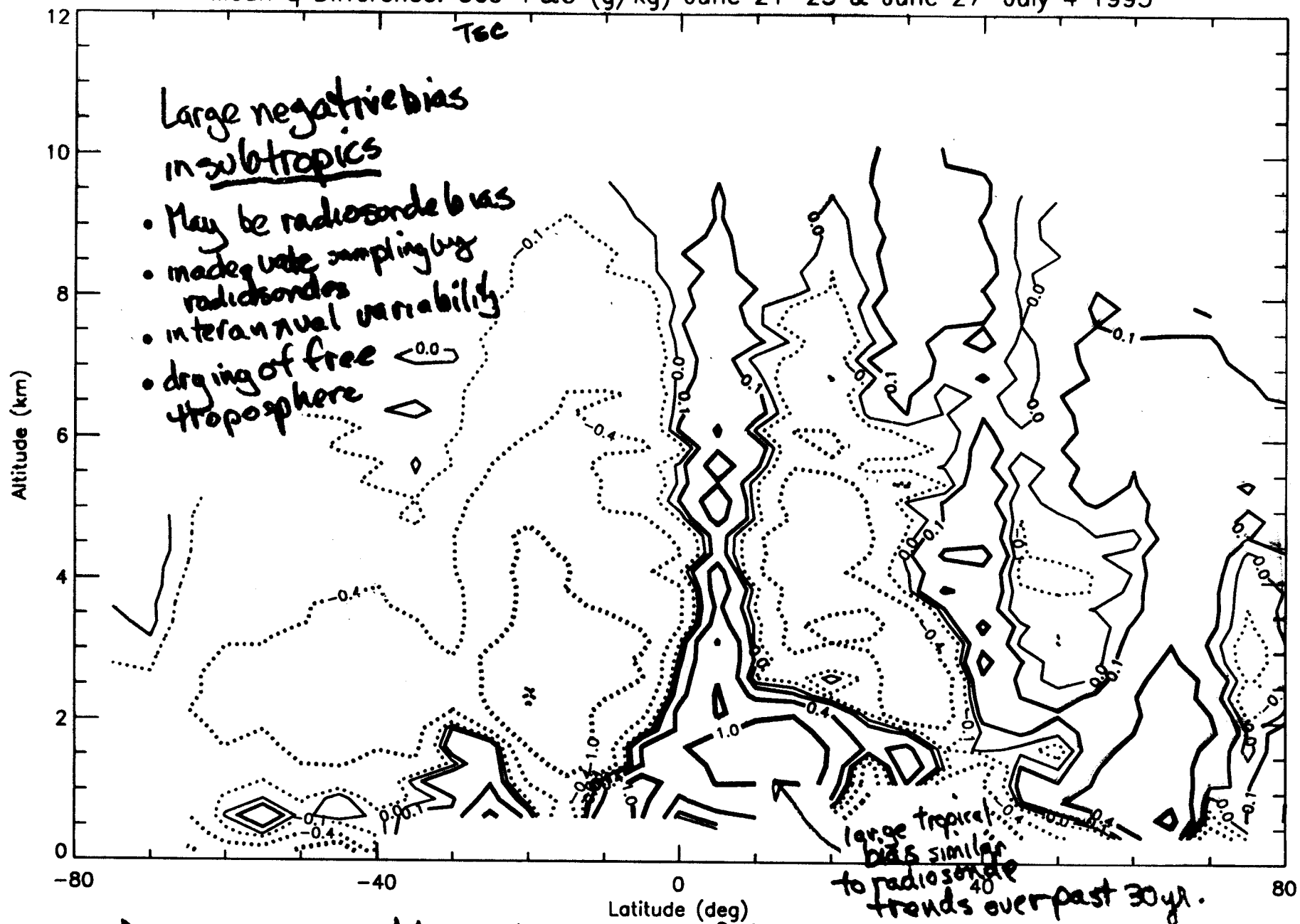
Mean Specific Humidity Difference: Occ-NCEP (g/kg) June 21-23 & June 27-July 4 1995



DIFFERENCE OF WATER VAPOR MIXING RATIO (g/kg)
 $q_{Occ} - q_{NCEP}$ REANALYSIS

KURASHIKA

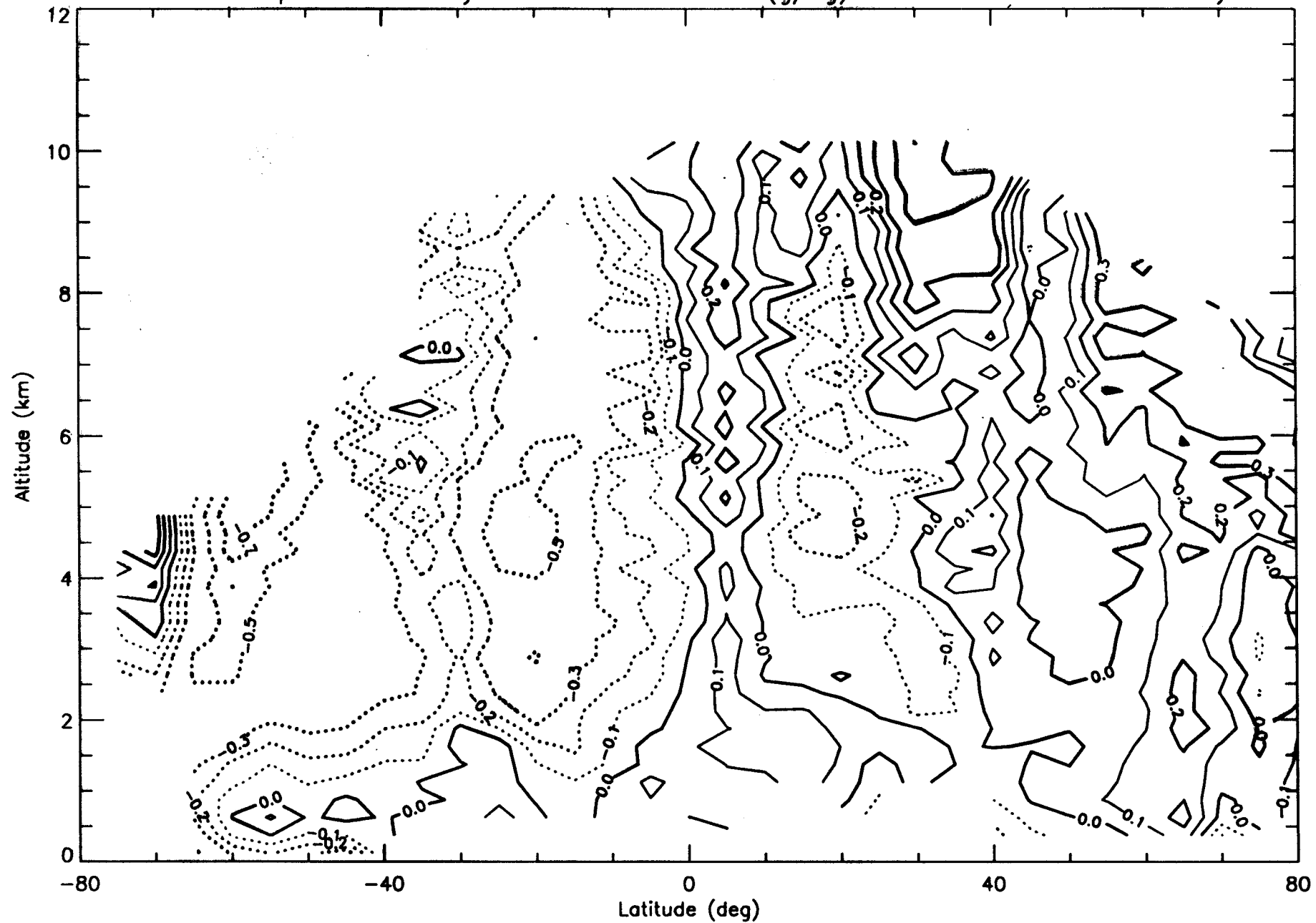
Mean q Difference: Occ-P&O (g/kg) June 21-23 & June 27-July 4 1995



Difference of Mean Water Vapor Mixing Ratio

GPS (6/21/95 - 7/4/95) — Peixoto: OORT JUN2-JULY-AUGUST 1963-1973
(radiosonde)

Normalized Mean Specific Humidity Difference: Occ-P&O (g/kg) June 21–23 & June 27–July 4 199



Kursinski & Hajj 1999

Separation of True Variability and Errors

Each observation can be decomposed into a true value plus an error such that the q from ECMWF ($\equiv q_E$) and that derived from GPS refractivity plus the ECMWF temperatures ($\equiv q_G$) can be written as

$$q_E = \bar{q} + q' + \overline{\varepsilon}_E + \varepsilon'_E$$

$$q_G = \bar{q} + q' + \overline{\varepsilon}_G + \varepsilon'_G$$

where ε_E and ε_G are the errors in the q_E and q_G estimates and overbars and primes refer to the zonal mean and variable parts of each term respectively.

The difference between the q estimates ($\equiv \Delta q$) is

$$\Delta q = q_G - q_E = \overline{\varepsilon}_G + \varepsilon'_G - \overline{\varepsilon}_E - \varepsilon'_E$$

The variance of the ECMWF and GEW q estimates and their differences can be written as

$$\sigma_{qE}^2 = \bar{q}'^2 + 2 \bar{q}'\bar{\epsilon}'_E + \bar{\epsilon}'_E^2 \quad (1a)$$

$$\sigma_{qG}^2 = \bar{q}'^2 + 2 \bar{q}'\bar{\epsilon}'_G + \bar{\epsilon}'_G^2 \quad (1b)$$

$$\sigma_{\Delta q}^2 = \bar{\epsilon}'_G^2 - 2 \bar{\epsilon}'_G \bar{\epsilon}'_E + \bar{\epsilon}'_E^2 \quad (1c)$$

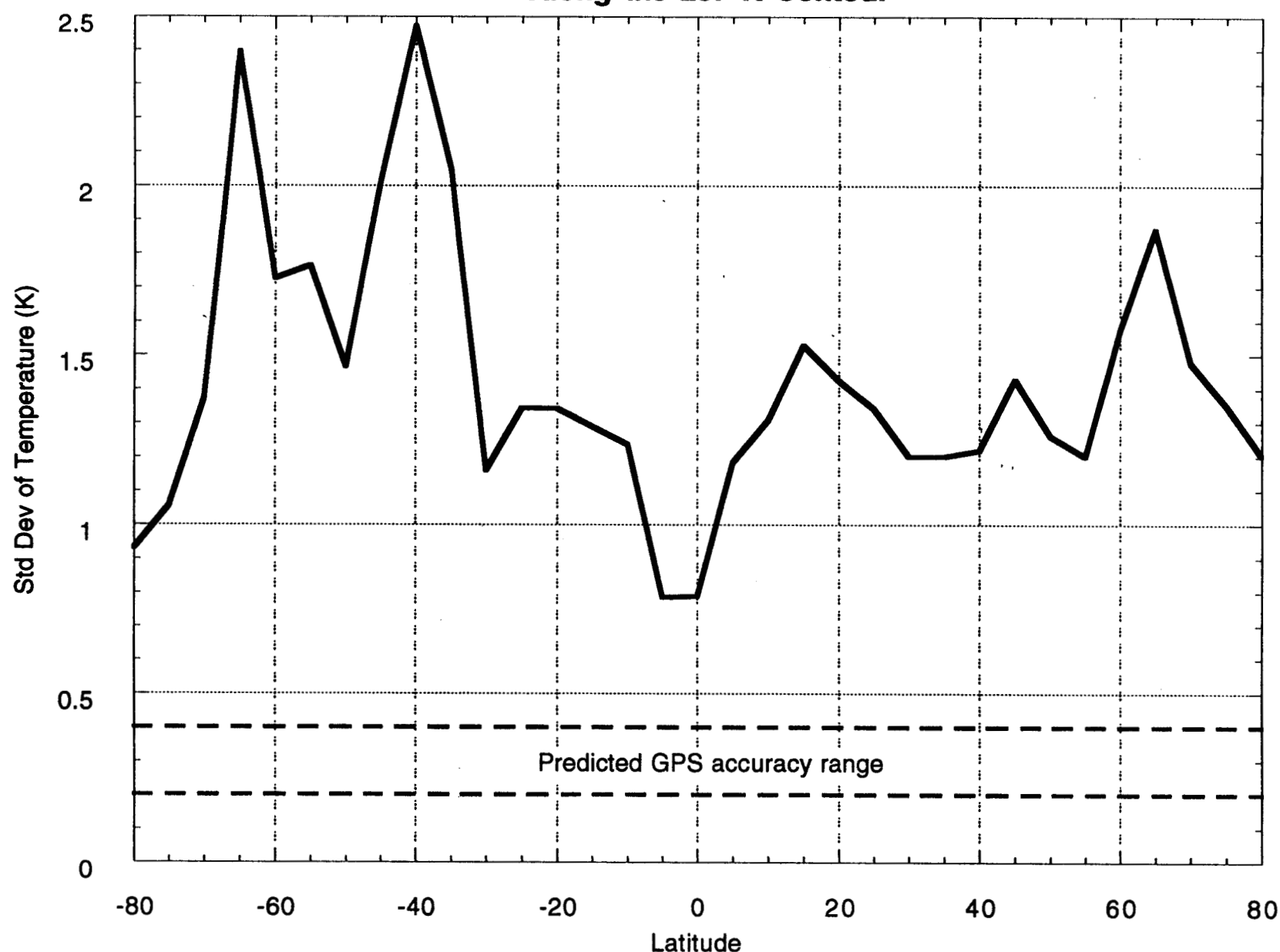
(1a-c) provide three constraints sufficient to isolate the true variability, the error in the q_G estimates and the error in the q_E estimates **if the correlation terms are small**. The three combinations which would do so are

$$\frac{1}{2}(\sigma_{qE}^2 + \sigma_{qG}^2 - \sigma_{\Delta q}^2) = \bar{q}'^2 + \bar{q}'\bar{\epsilon}'_E + \bar{q}'\bar{\epsilon}'_G + \bar{\epsilon}'_E \bar{\epsilon}'_G \quad (2a)$$

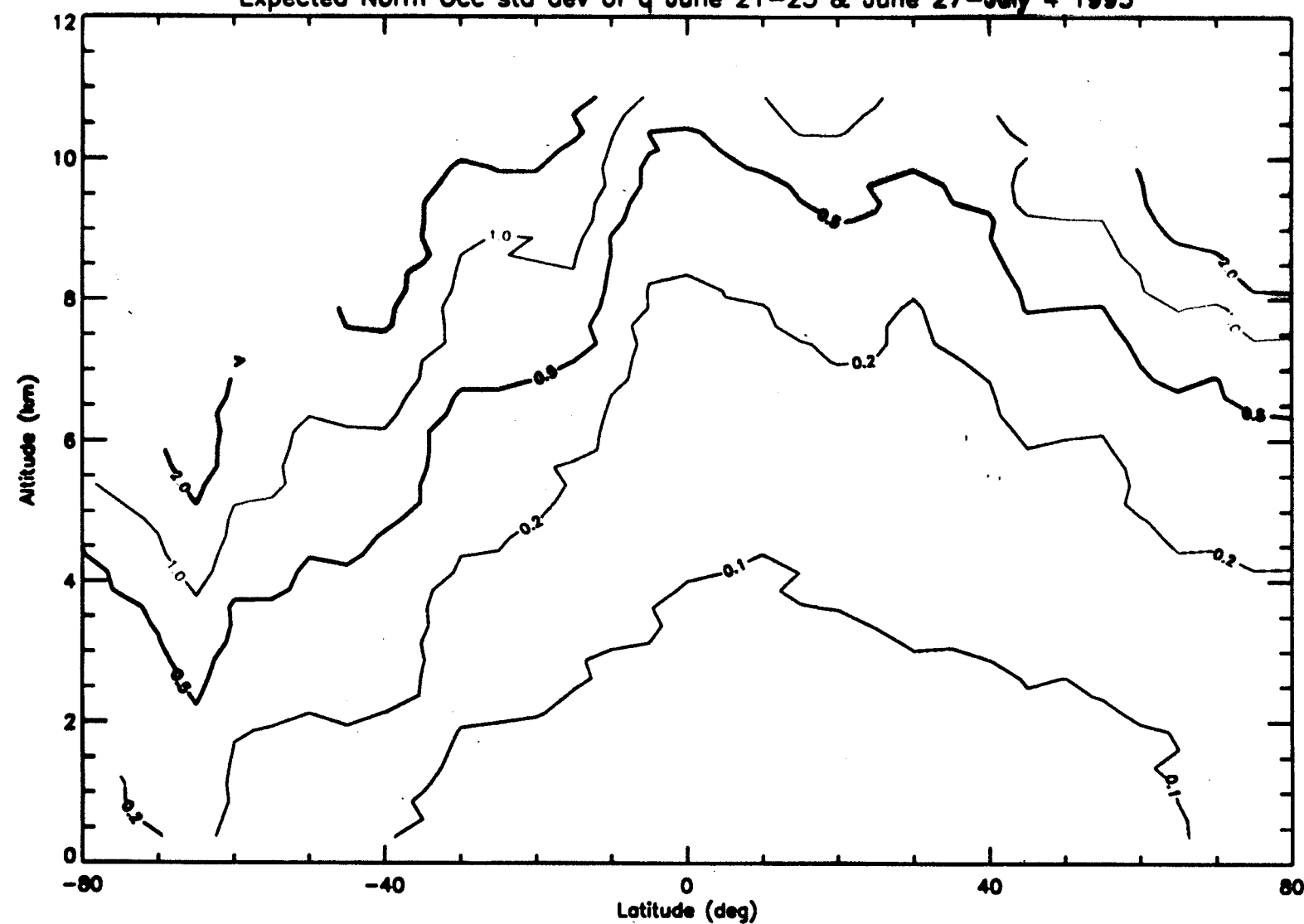
$$\frac{1}{2}(\sigma_{qE}^2 - \sigma_{qG}^2 + \sigma_{\Delta q}^2) = \bar{\epsilon}'_E^2 + \bar{q}'\bar{\epsilon}'_E - \bar{q}'\bar{\epsilon}'_G - \bar{\epsilon}'_E \bar{\epsilon}'_G \equiv L_E \quad (2b)$$

$$\frac{1}{2}(-\sigma_{qE}^2 + \sigma_{qG}^2 + \sigma_{\Delta q}^2) = \bar{\epsilon}'_G^2 - \bar{q}'\bar{\epsilon}'_E + \bar{q}'\bar{\epsilon}'_G - \bar{\epsilon}'_E \bar{\epsilon}'_G \equiv L_G \quad (2c)$$

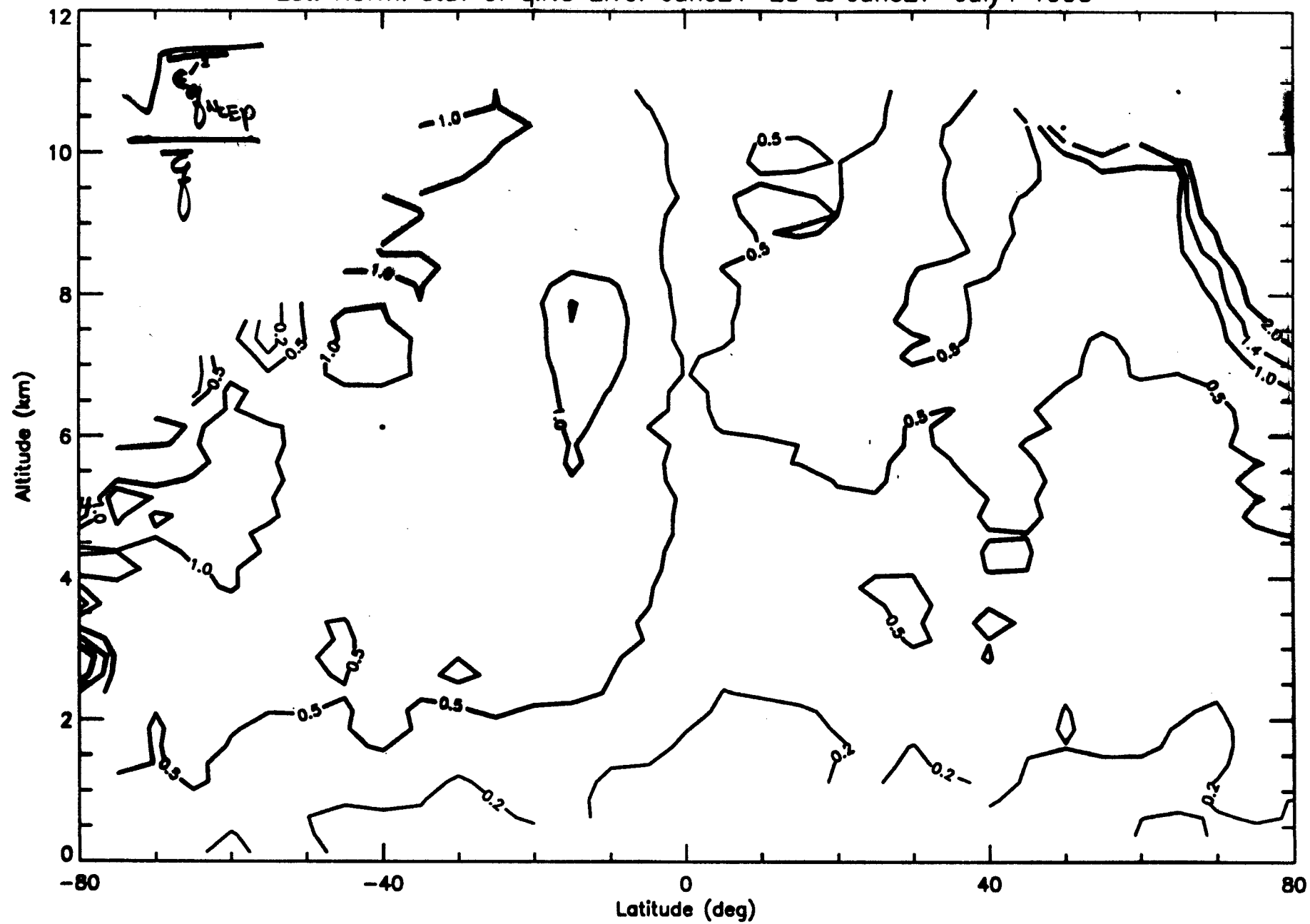
**Standard Deviation of Temperature Differences
Between GPS Occultations and ECMWF Analyses
Along the 237 K Contour**



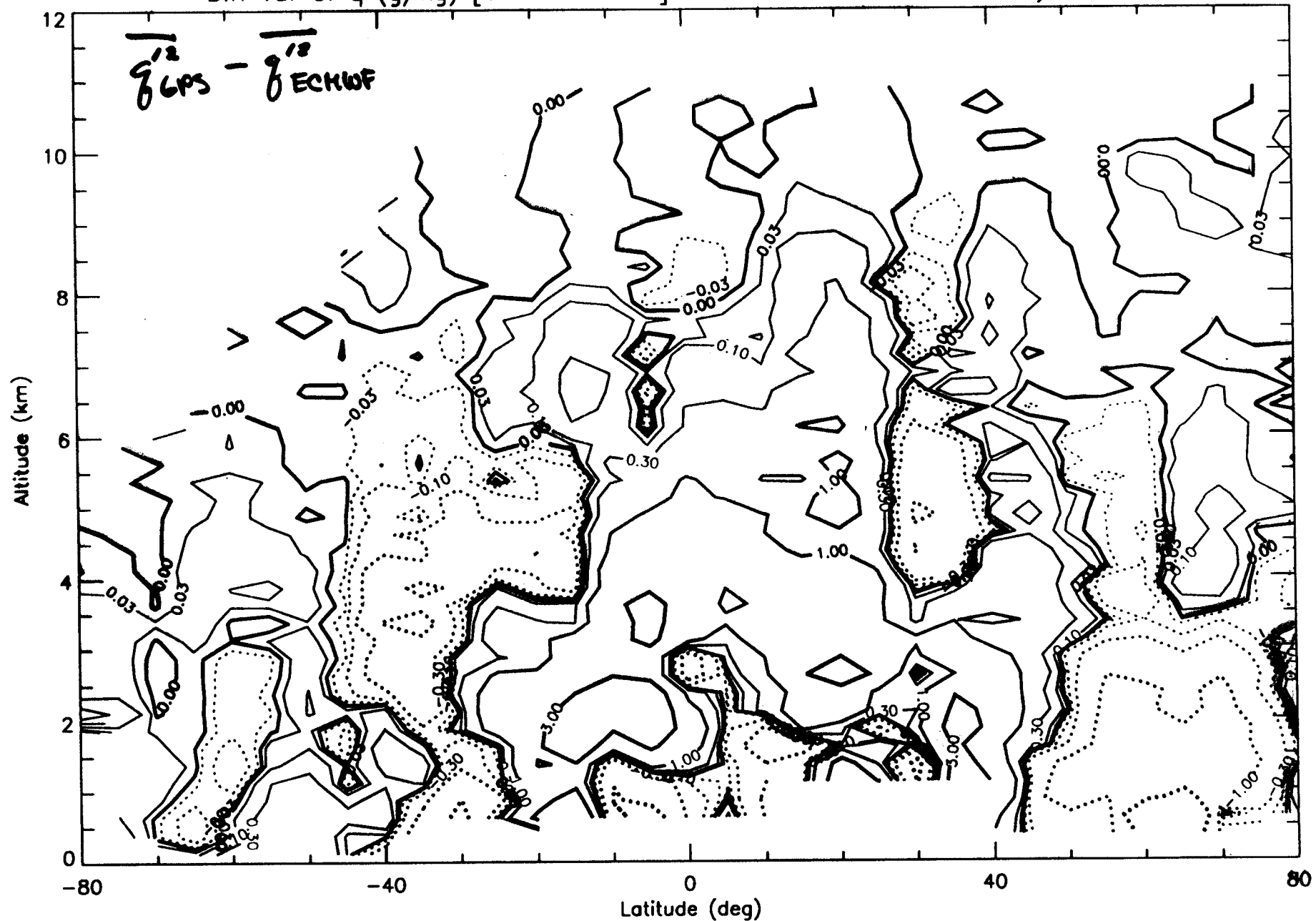
Expected Norm Occ std dev of q June 21-23 & June 27-July 4 1995



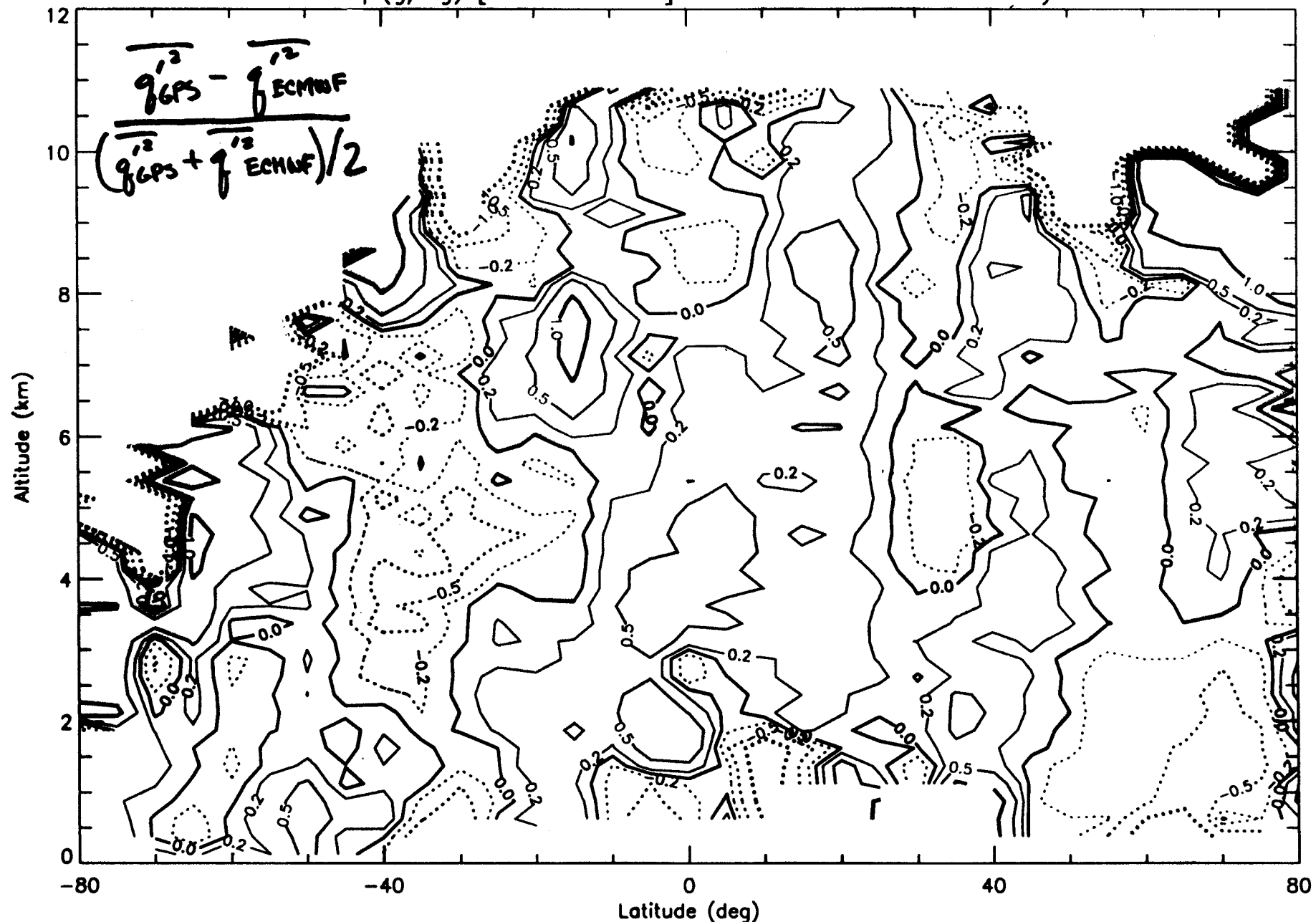
Est. Norm. stdv of qINC Error June21–23 & June27–July4 1995



Diff var of q (g/kg) [Occ - ECMWF] June 21-23 & June 27-July 4 1995

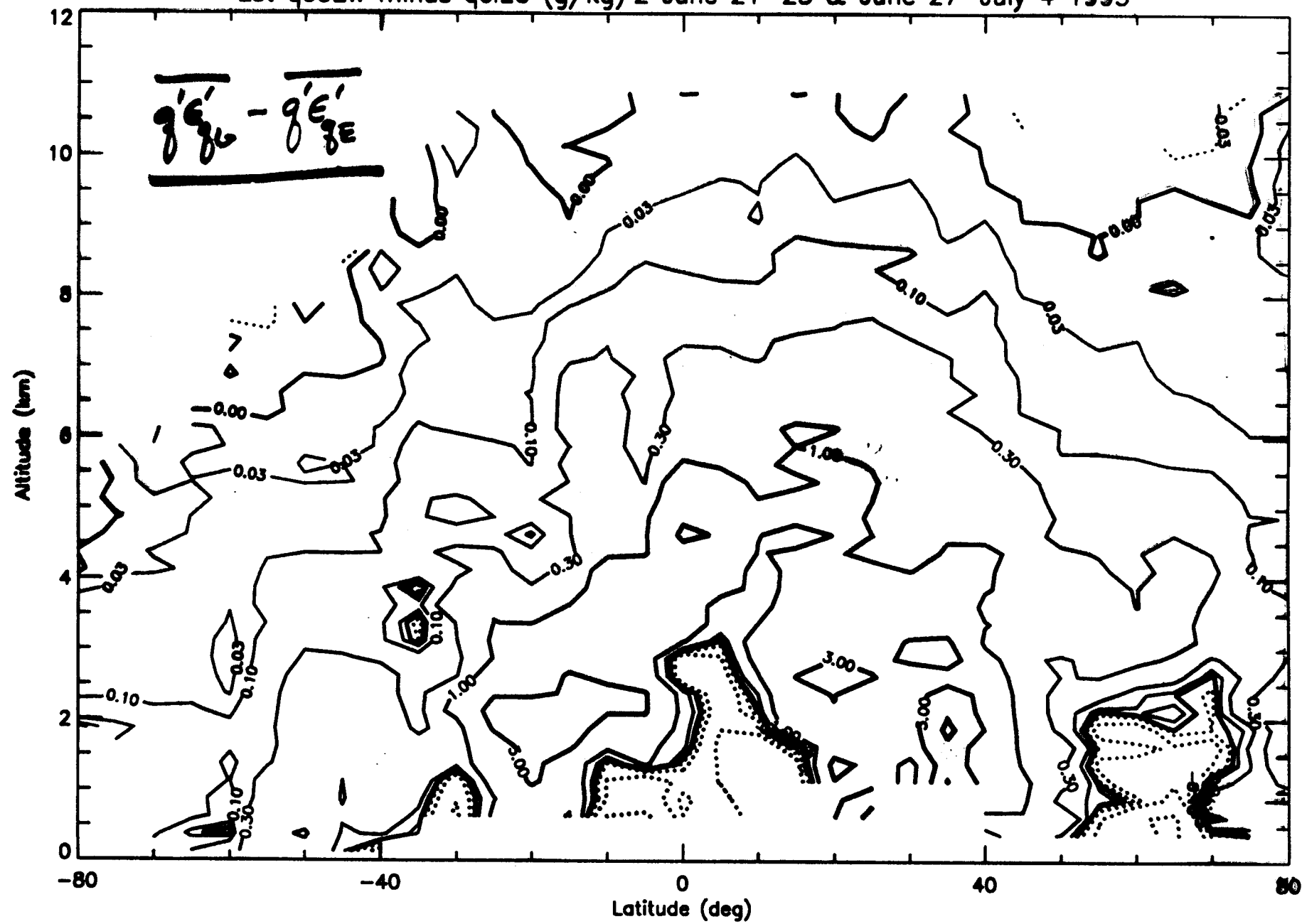


Diff var of q (g/kg) [Occ - ECMWF] June 21-23 & June 27-July 4 1995



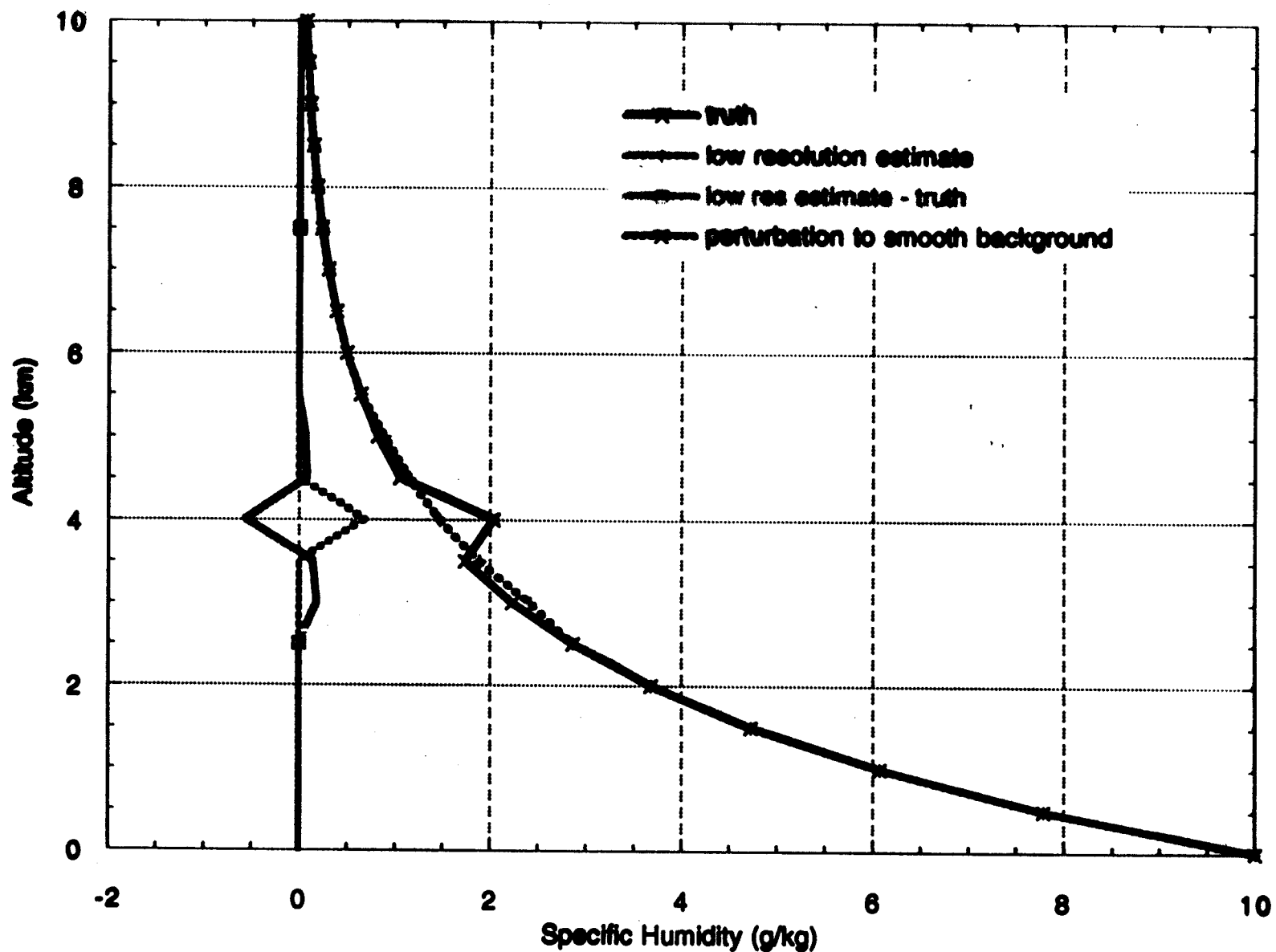
Kursinstskr! Hajj
5/99

Est q_{SEW} minus q_{EIC} (g/kg) 2 June 21-23 & June 27-July 4 1995



Kursinski & Hajj
5/99

**Negative Correlation Between Moisture Variations
and Low Resolution Estimate Error**



Kursinski? Hajj
5/99

Assimilation of GPS data into weather predictions and analyses (from Palmer, Barnett and Eyre, AMS conf. 1998)

Problem: How to use a set of measurements to improve the estimate of the atmospheric state in a model

Approach: Define a penalty function and minimize it by adjusting the model variables.

Assuming errors are Gaussian, the maximum likelihood penalty function is then

$$\xi(x) = \underbrace{(y_{obs} - y(x))^T S_y^{-1} (y_{obs} - y(x))}_{\text{observation part}} + \underbrace{(x - x_a)^T S_a^{-1} (x - x_a)}_{\text{model part}}$$

where: y_{obs} is the vector of measurements,

$y(x)$ is the simulated measurements based on the model state vector x ,

x_a is the apriori model state vector and S_a is its expected error covariance.

S_y is the measurement error covariance plus the covariance of the forward model.

Minimizing $\xi(x)$ means finding x such that

$$\nabla_x \xi(x) = S_a^{-1}(x - x_a) - K^T S_y^{-1} (y_{obs} - y(x)) = 0$$

where K is $\nabla_x y$.

$y(x)$ is in general nonlinear such that we must linearize $y(x)$ and iterate to find the solution which is

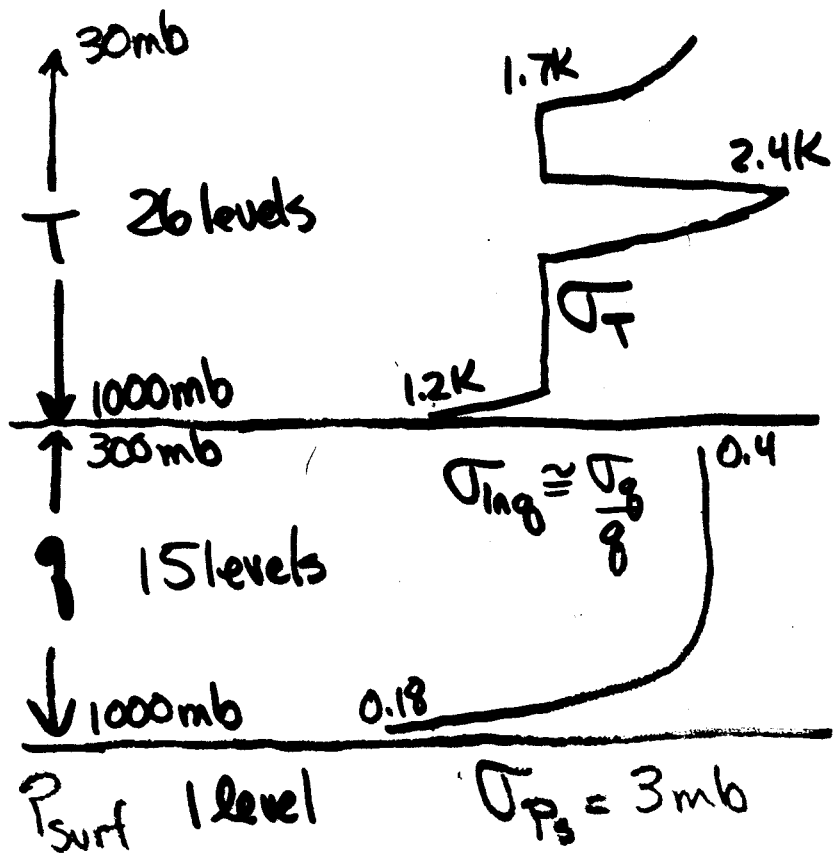
$$x_{n+1} = x_n - [H_x \xi(x)]^{-1} \nabla_x \xi(x_n)$$

where n is the iteration index and H is the Hessian operator which is obtained by differentiating $\nabla_x \xi(x_n)$ again:

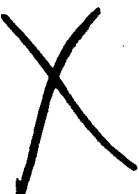
$$H_x \xi(x) \equiv S_a^{-1} + K^T S_y^{-1} K$$

The error covariance of x is

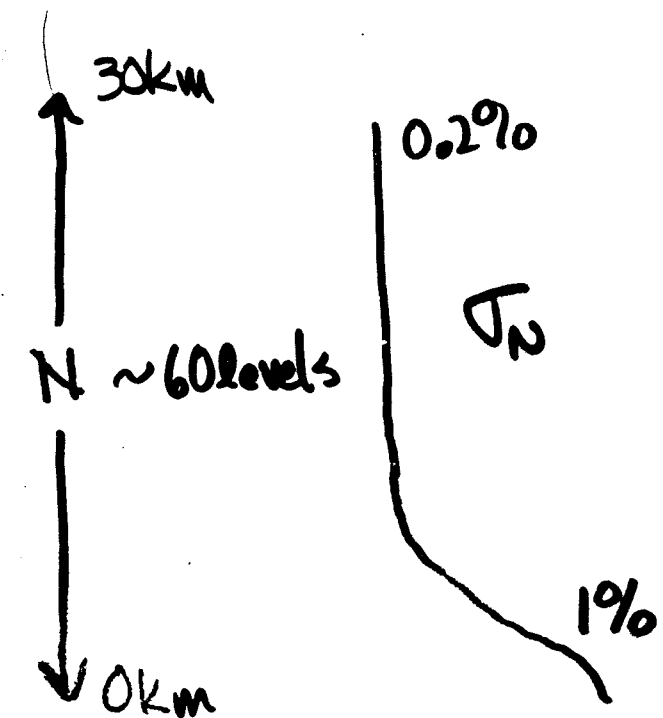
$$\hat{S} = \underline{\underline{[S_a^{-1} + K^T S_y^{-1} K]^{-1}}}$$



Model State
Vector
 $\equiv \mathbf{x}$ solution
 $\equiv \mathbf{x}_a$ apriori



Diagonal
Terms of
 S_x

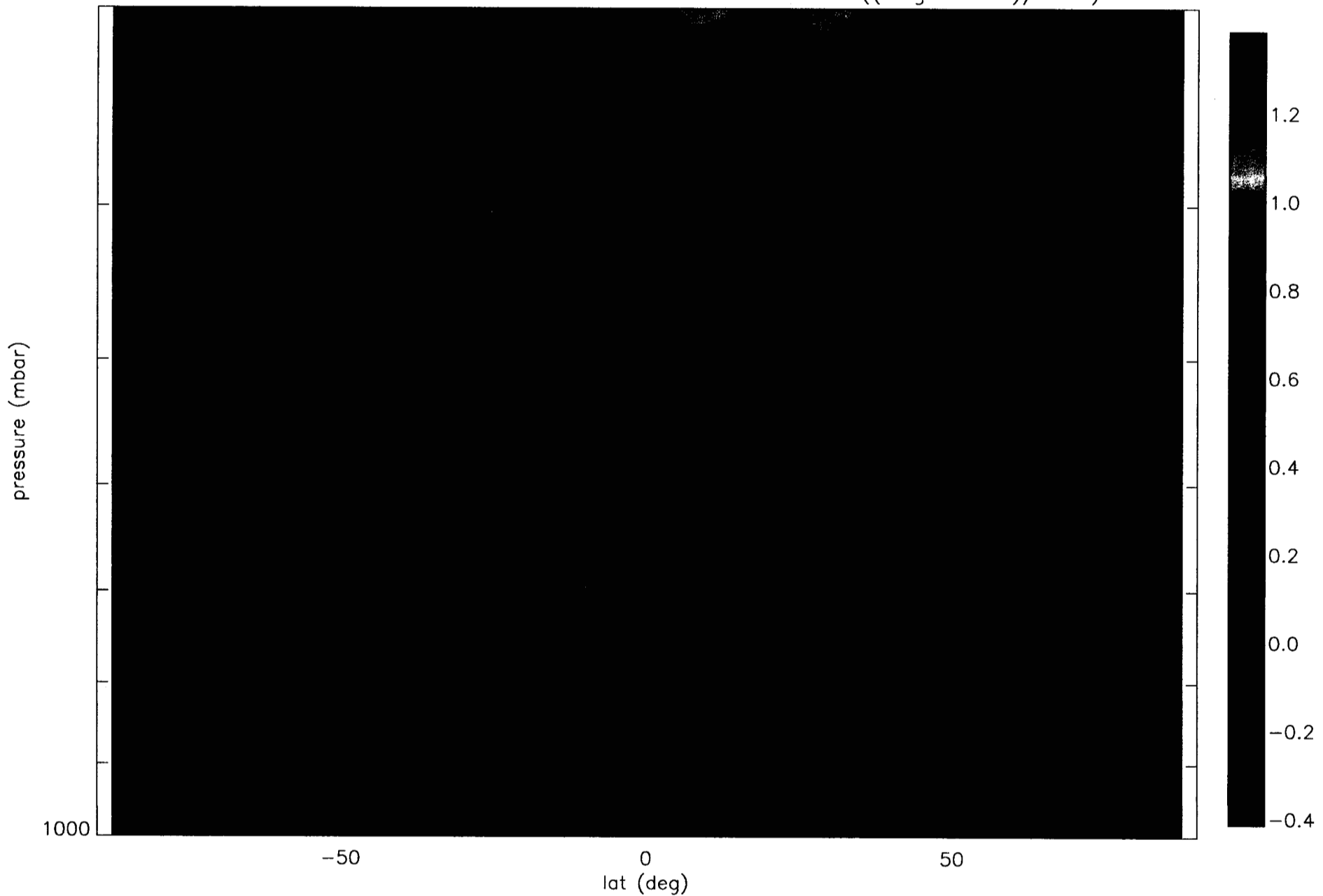


Observation
Vector
 $\equiv \mathbf{y}$

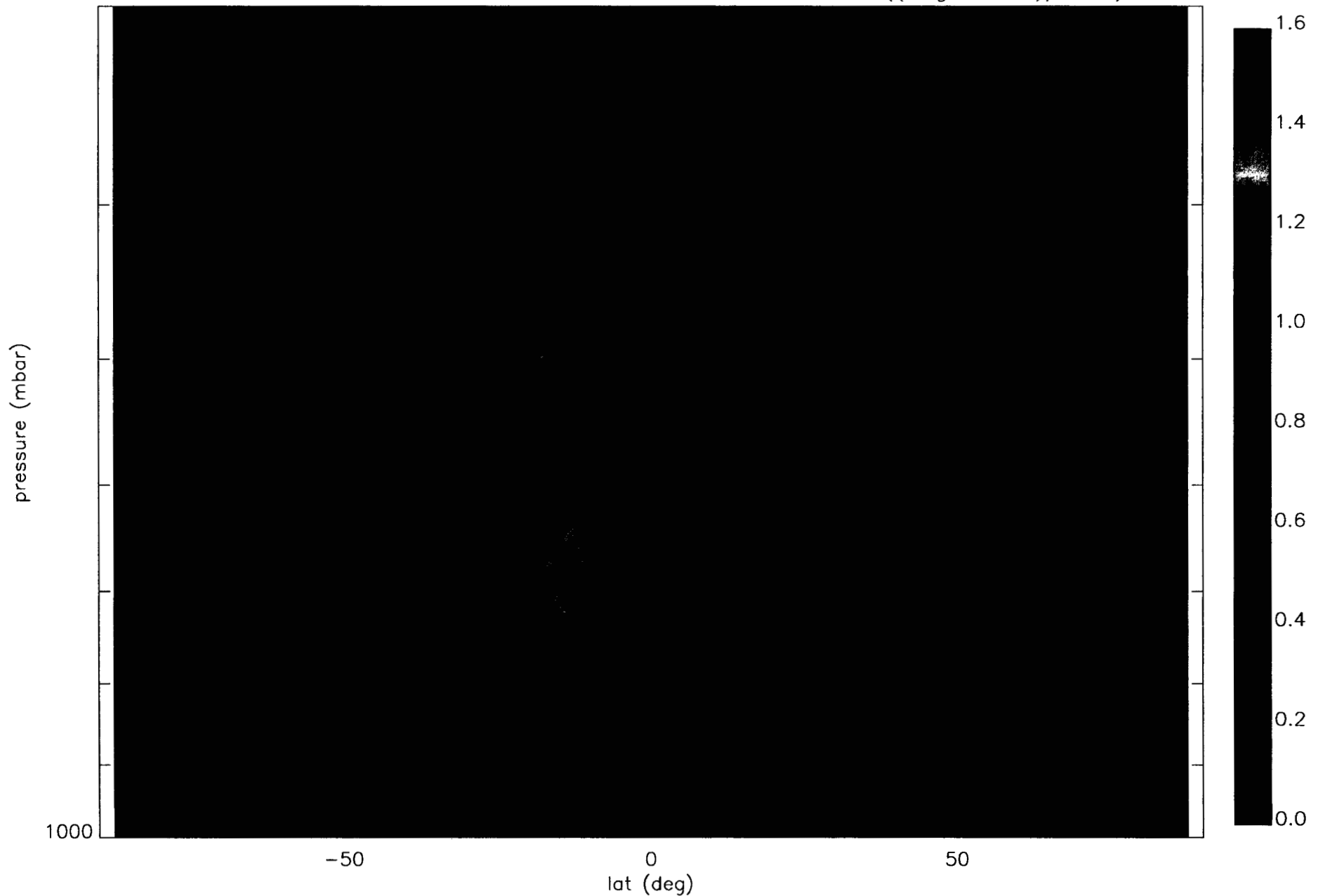


Diagonal
Terms of
 S_y

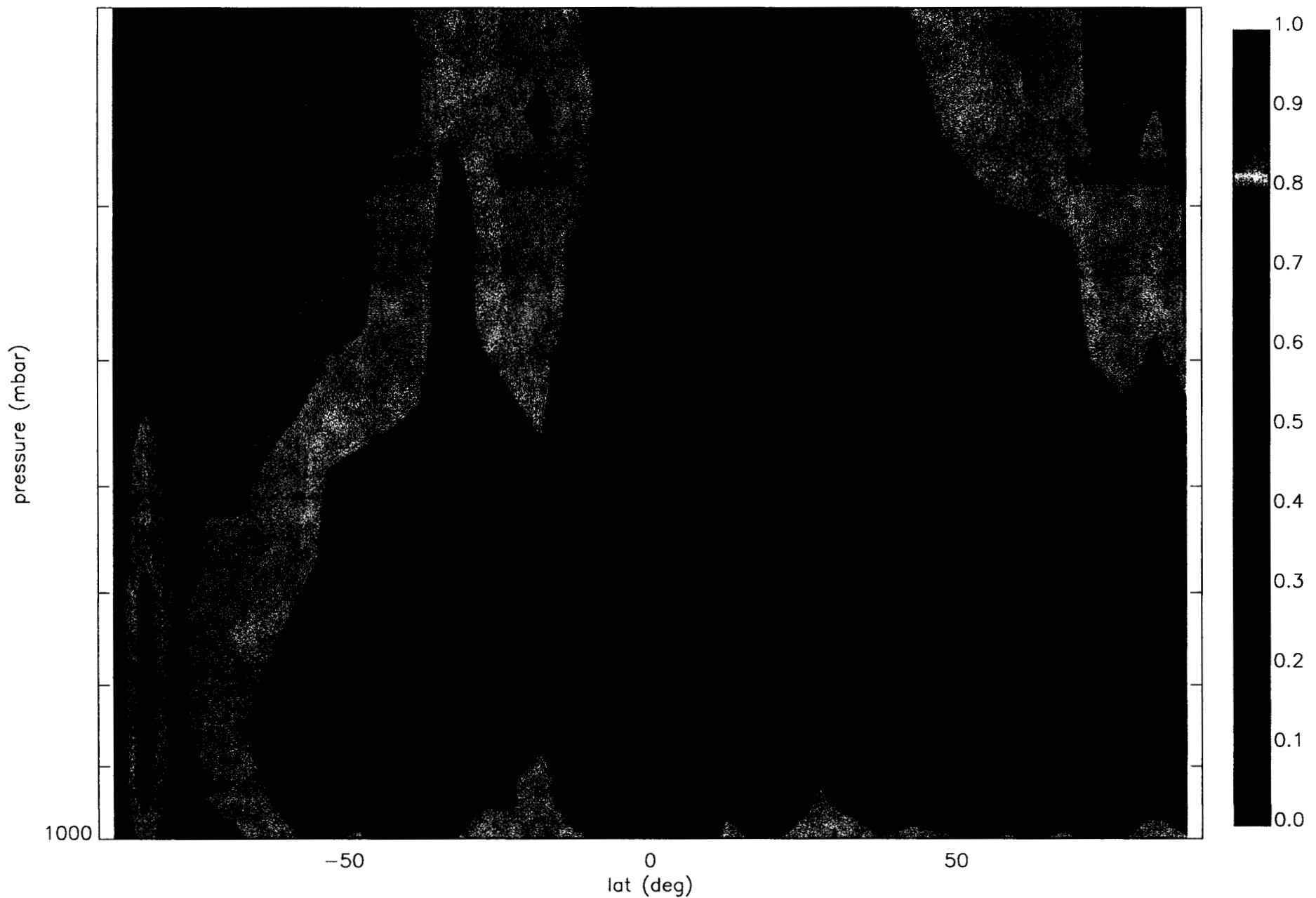
MEAN OF SPECIFIC HUMIDITY FRACTIONAL DIFFERENCE ((Bkgd-Soln)/Soln)



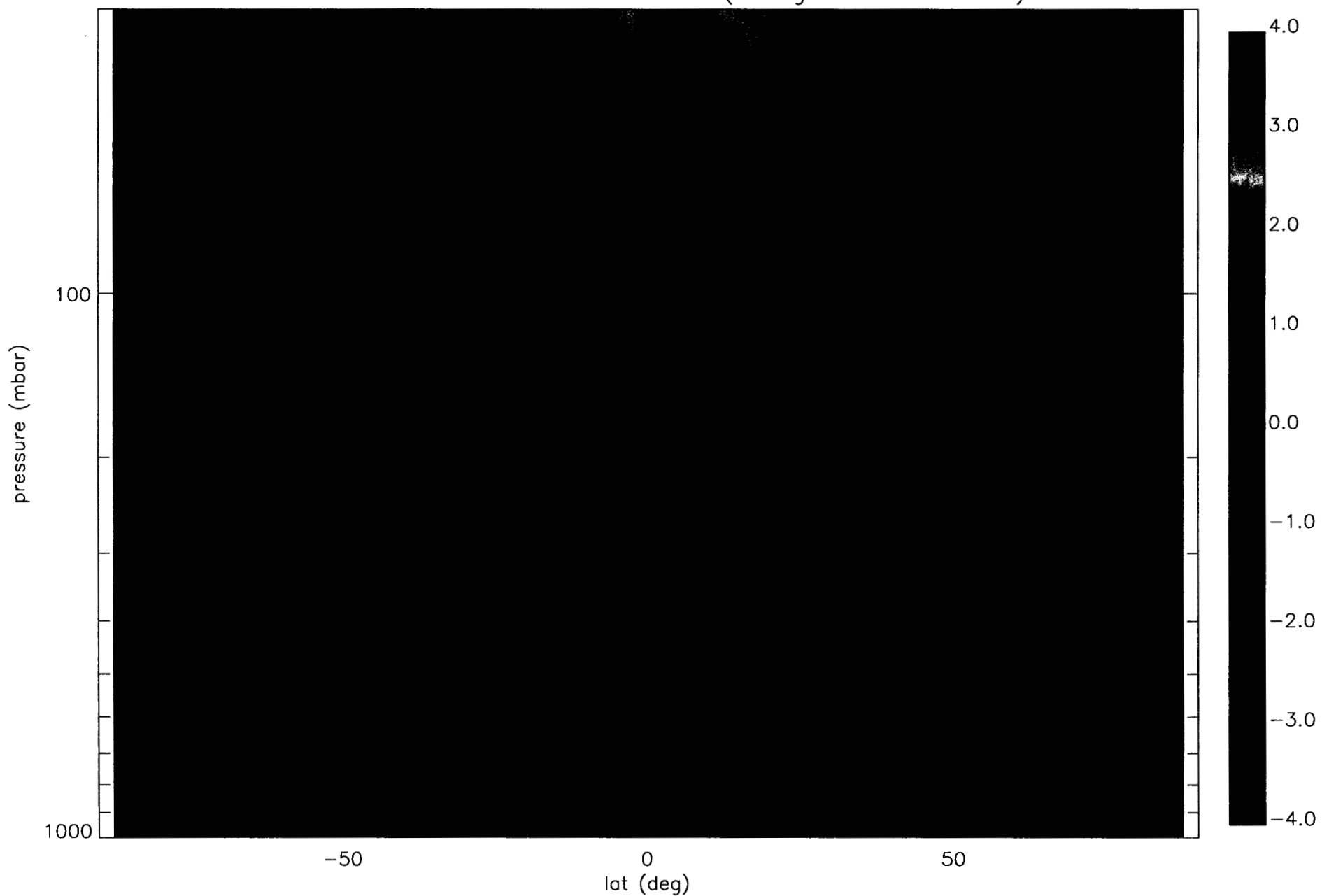
STD.DEV. OF SPECIFIC HUMIDITY FRACTIONAL DIFFERENCE ((Bkgd-Soln)/Soln)



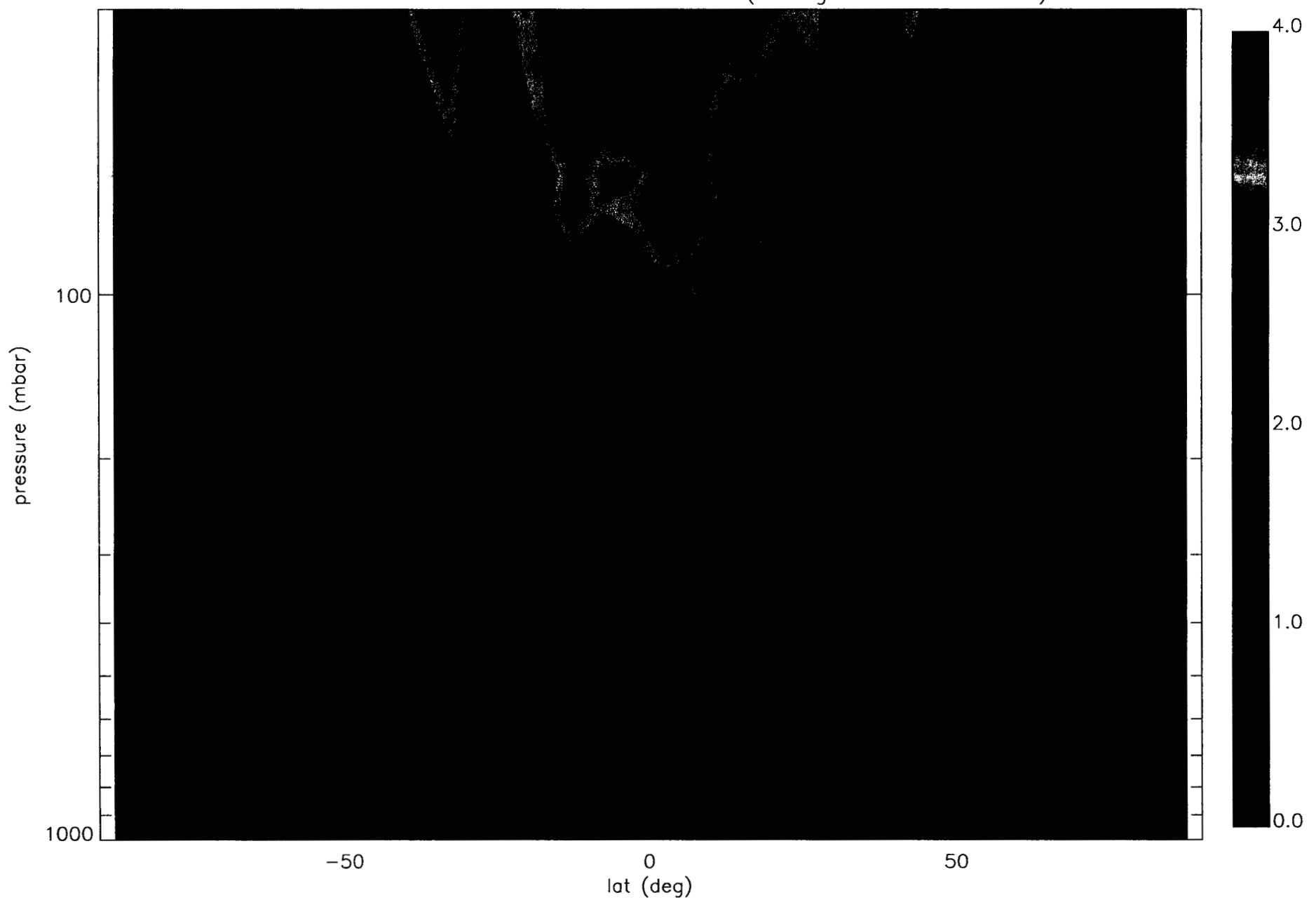
SPECIFIC HUMIDITY IMPROVEMENT
 $\text{sqrt}(\text{var solution}/\text{var background})$

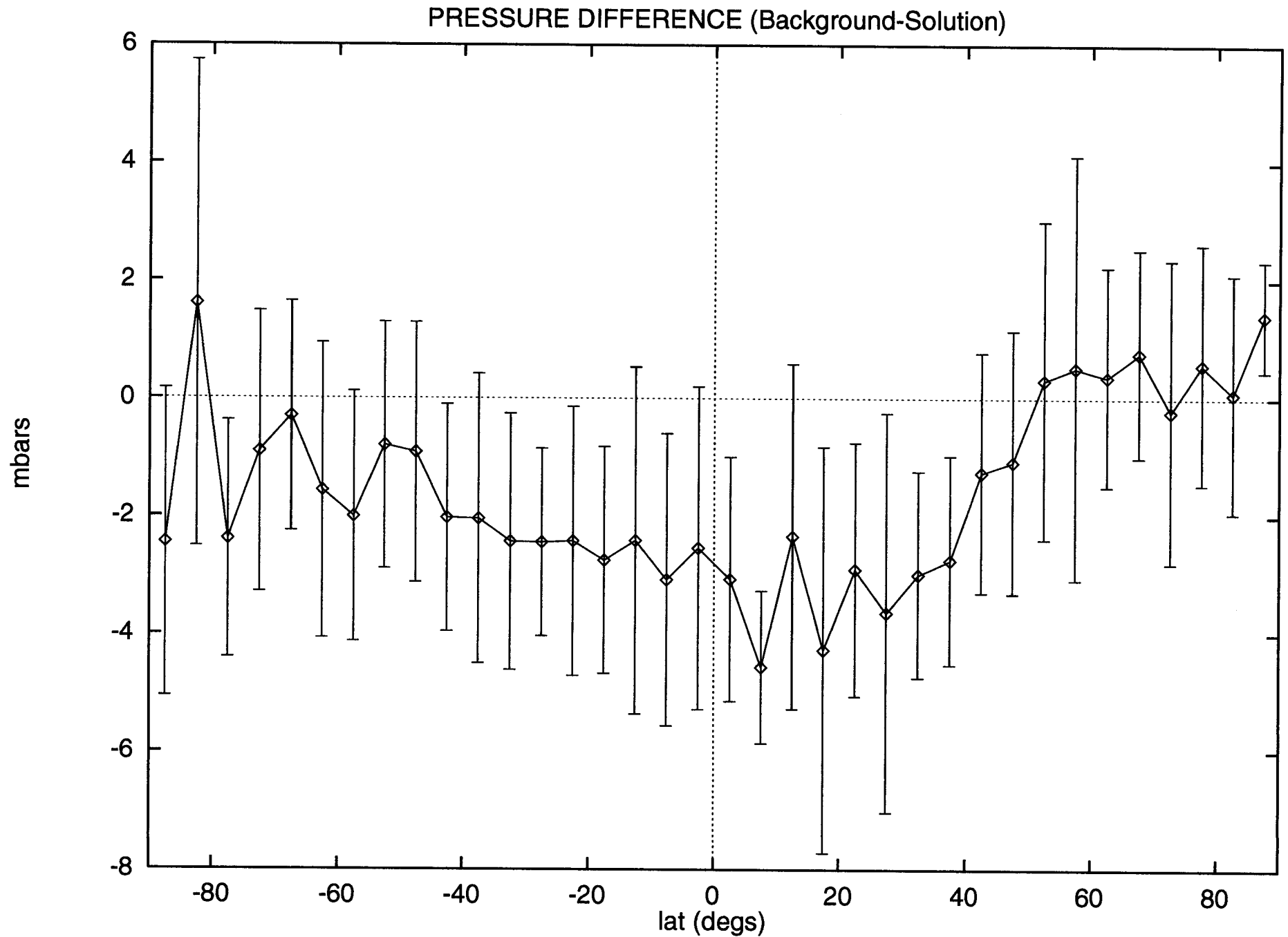


MEAN OF TEMPERATURE DIFFERENCE (Background – Solution)

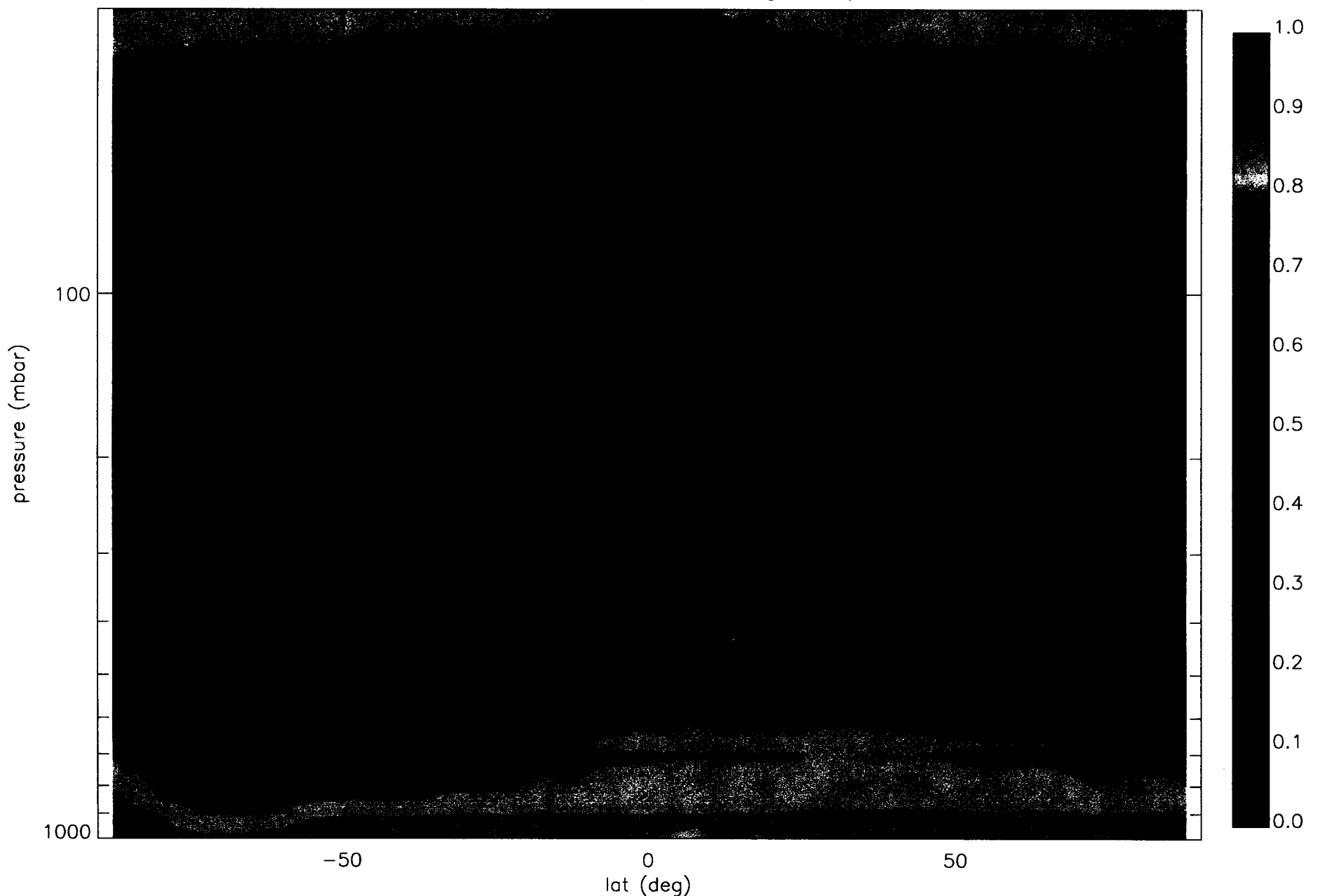


STD.DEV. OF TEMPERATURE DIFFERENCE (Background – Solution)

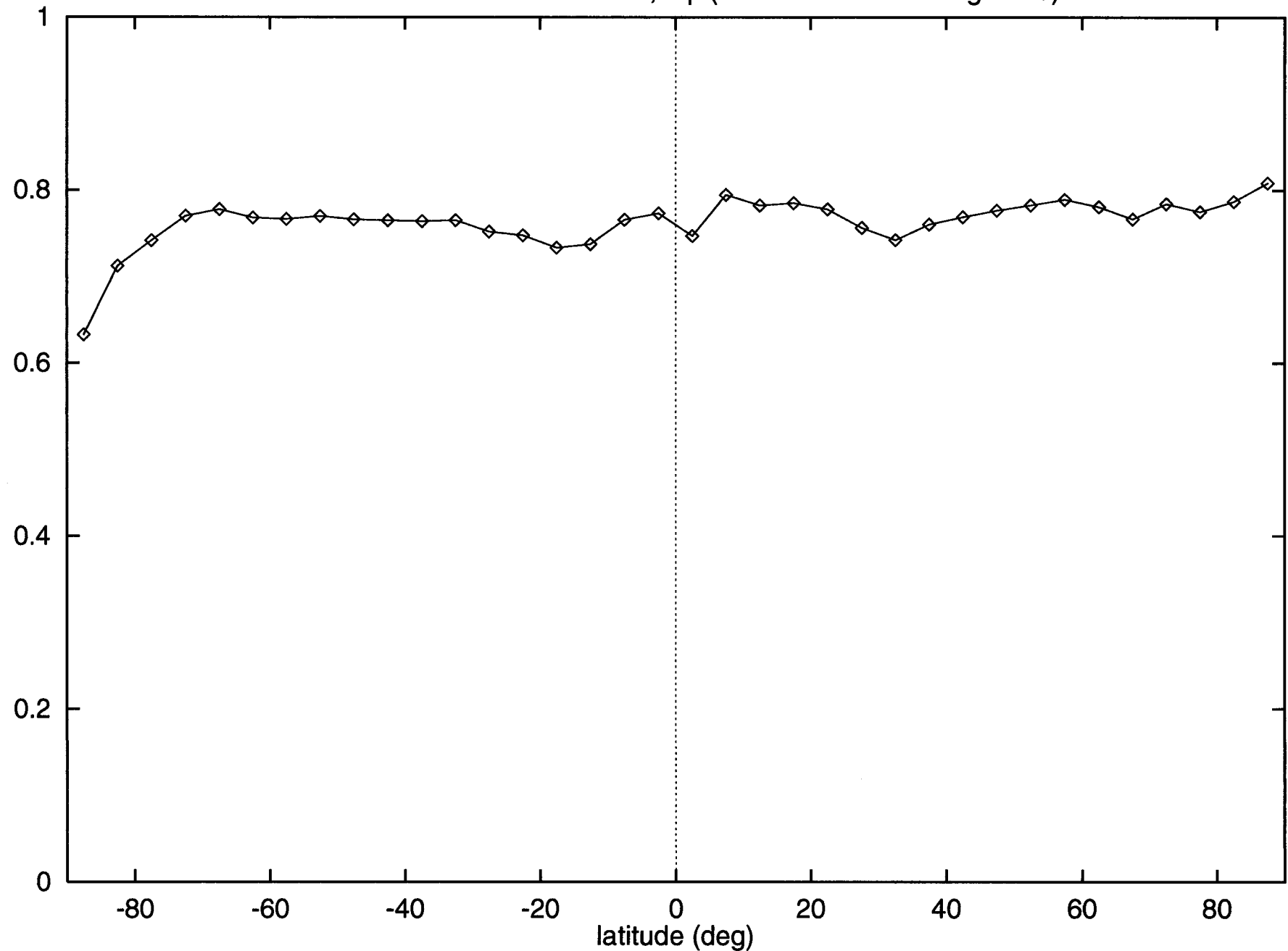




TEMPERATURE IMPROVEMENT
 $\text{sqrt}(\text{var solution}/\text{var background})$



PRESSURE IMPROVEMENT, $\text{sqrt}(\text{var solution}/\text{var background})$



Conclusions / Summary

Occultations yield specific (not relative) humidity

$$\bar{T}_q \sim 0.2 \text{ to } 0.5 \text{ g/kg}, \quad \bar{E}_q \sim 0.1 \text{ g/kg}$$

Zonal mean moisture examination June 21 - July 4, 1995

ECHWF analyses too moist below $\sim 400 \text{ mb}$

NCEP reanalyses similar but also too dry at ITCZ

ECHWF drier and colder than NCEP above 400 mb

Peixoto; Oort is biased moist in subtropics, dry in ITCZ
(due to...?)

Conclusions / Summary

1DVar using occultation refractivity and ECMWF analyses

- Framework is simple
- Results are preliminary because covariances are not right
 - initially χ^2 are within \sim factor of 2
 - covariances are not terrible
- Covariance improvements
 - Single, global covariances are inadequate
 - Tcovar increased in tropical, lower stratosphere
 - Tcovar needs to reflect variation in tropopause with latitude
 - qcovar needs to be increased in subtropics
 - Ncovar needs to reflect dependence on horizontal structure
- Comments on Impact on model state vector
 - Impact is under estimated due to covariance errors.
 - Is surface pressure adjustment real? may be a gravity error?
 - Tropospheric lapse rates are being adjusted
 - presumably to get lower stratosphere densities to match N's